Title

Cortical interlaminar astrocytes across the therian mammal radiation

Journal

The Journal of Comparative Neurology, 527(10)

ISSN

1550-7149

Authors

Falcone, Carmen
Wolf-Ochoa, Marisol
Amina, Sarwat
et al.

Publication Date

2019-07-01

DOI

10.1002/cne.24605

Peer reviewed

HHS Public Access

Author manuscript

J Comp Neurol. Author manuscript; available in PMC 2020 January 01.

Published in final edited form as:

J Comp Neurol. 2019 July 01; 527(10): 1654–1674. doi:10.1002/cne.24605.

Cortical interlaminar astrocytes across the therian mammal radiation

Carmen Falcone[1,2], **Marisol Wolf-Ochoa**[1,2], **Sarwat Amina**[2,3], **Tiffany Hong**[1,2], **Gelareh Vakilzadeh**[1,2], **William D. Hopkins**[4], **Patrick R. Hof**[5], **Chet C. Sherwood**[6], **Paul R. Manger**[7], **Stephen C. Noctor**[3,8], and **Verónica Martínez-Cerdeño**[1,2,3]

[1]Department of Pathology and Laboratory Medicine, UC Davis School of Medicine, Sacramento, California

[2]Institute for Pediatric Regenerative Medicine, Shriners Hospitals for Children of Northern California, Sacramento, California

[3]UC Davis Medical Center, MIND Institute, Sacramento, California

[4]Neuroscience Institute and Language Research Center, Georgia State University, Atlanta, Georgia

[5]Fishberg Department of Neuroscience and Friedman Brain Institute, Icahn School of Medicine at Mount Sinai, New York, New York

[6]Department of Anthropology and Center for the Advanced Study of Human Paleobiology, The George Washington University, Washington, DC

[7]School of Anatomical Sciences, Faculty of Health Sciences, University of the Witwatersrand, Johannesburg, South Africa

[8]Department of Psychiatry and Behavioral Sciences, UC Davis School of Medicine, Sacramento, California

Abstract

Interlaminar astrocytes (ILA) in the cerebral cortex possess a soma in layer I and extend an interlaminar process that runs perpendicular to the pia into deeper cortical layers. We examined cerebral cortex from 46 species that encompassed most orders of therian mammalians, including 22 primate species. We described two distinct cell types with interlaminar processes that have been referred to as ILA, that we termed pial ILA and supial ILA. ILA subtypes differ in somatic morphology, position in layer I, and presence across species. We further described *rudimentary* ILA that have short GFAP$^+$ processes that do not exit layer I, and "typical" ILA with longer GFAP$^+$ processes that exit layer I. Pial ILA were present in all mammalian species analyzed, with typical ILA observed in Primates, Scandentia, Chiroptera, Carnivora, Artiodactyla, Hyracoidea, and Proboscidea. Subpial ILA were absent in Marsupialia, and typical subpial ILA were only found in Primate. We focused on the properties of pial ILA by investigating the molecular properties of pial ILA and confirming their astrocytic nature. We found that while the density of pial ILA somata

Correspondence: Verónica Martínez-Cerdeño, 2425 Stockton, Boulevard, Sacramento, California, 95817., vmartinezcerdeno@ucdavis.edu.

only varied slightly, the complexity of ILA processes varied greatly across species. Primates, specifically bonobo, chimpanzee, orangutan, and human, exhibited pial ILA with the highest complexity. We showed that interlaminar processes contact neurons, pia, and capillaries, suggesting a potential role for ILA in the blood-brain barrier and facilitating communication among cortical neurons, astrocytes, capillaries, meninges, and cerebrospinal fluid.

Keywords

astrocyte; cerebral cortex; evolution; human; mammal; primate; RRID:AB_10013382; RRID:AB_2057371; RRID:AB_91530; RRID:SCR_001775; RRID:SCR_002285; RRID:AB_477010; RRID:AB_839504; RRID:AB_443209; RRID:AB_776174; RRID:AB_2298772; RRID:AB_570666; RRID:AB_882426; RRID:AB_778021; RRID:AB_141708; RRID:AB_141633; RRID:AB_2313663; RRID:AB_2313574; RRID:AB_2340593

1 | INTRODUCTION

William Lloyd Andriezen was the first to describe interlaminar astrocytes (ILA), which he initially called *caudate neuroglial fiber cells* in a 1893 paper that reported the characteristics of neuroglia elements in the human brain (Andriezen, 1893), (Figure 1a). Golgi stained samples of human cortex revealed long, smooth, unbranched processes that were slightly wavy and exhibited occasional small sharp curves and angular bends. These processes did not anastomose and did not show any vascular connection. Several of these processes originated from somata that were located within layer I of the cerebral cortex and were characterized by an inverted pyramidal shape with a flat base contacting the pia. Andriezen also described two additional fiber types originating from these somata, a superficial tangential system of fibers that formed a true felt-work, and a few shorter fibers passing to the superjacent pia. He described the absence of these cells in the cortices of cat, rabbit, ox, and rat. Within 1 year (1894), Ramón y Cajal and Retzius included this newly described cell type in their drawings of the cerebral cortex, showing cells with the same inverted pyramidal morphology and multiple unbranched processes (Figure 1b,c). In addition, Cajal included in some of his drawings a cell type that also had interlaminar processes but had a distinct morphology and position: these cells had a round soma, were located in the upper half of layer I, did not contact the pia, but extended 2–4 short processes that contacted the pia matter.

Nearly 100 years passed before the work of Jorge *A. Colombo* examined and described more about these unique cells. He first presented on these cells at a European Meeting, when he referred to them as *transitional glia* in adult *Cebus apella* cortex (Colombo & Puissant, 1994). One year later, he used the term *interlaminar astroglial processes* for glial fibriliary acidic protein (GFAP) immunoreactive ($^+$) long cellular processes originating in cortical layer I and traversing several cortical laminae, both in the prefrontal and rostral cingulate cortices in two adult New World monkey species, *Cebus apella* and *Saimiri sciureus* (Colombo, Yáñez, Puissant, & Lipina, 1995). He also described that these GFAP$^+$ processes were not present in rats (Colombo, 1996). In 1997, Colombo performed electron microscopy in frontal and temporal cerebral cortices obtained from five human patients who underwent brain surgery. He observed GFAP$^+$ interlaminar processes that were 300–500 μm-long, and

that had club-like endings that enclosed GFAP$^+$ intermediate filaments, mitochondria, and electron-dense material (Colombo, Gayol, Yáñez, & Marco, 1997). He suggested that the long processes represent a predominant characteristic in postnatal primate cerebral cortex (Colombo, Lipina, Yáñez, & Puissant, et al., 1997). Furthermore, he used the term "*palisade*" to describe an abundance of these long, densely-packed, radially distributed astroglial processes crossing several cortical laminae. He proposed that palisades could be instrumental to the columnar organization of the primate cerebral cortex (Colombo & Reisin, 2004). He published additional work describing the presence of these processes in many primate species and also in the lateral cortex of megachiropteran bat species and tree shrews (Colombo, Fuchs, Härtig, Marotte, & Puissant, 2000; Colombo, Härtig, Lipina, & Bons, 1998; Colombo, Sherwood, & Hof, 2004), and showed the postnatal origin of the interlaminar processes (Colombo, Lipina, et al., 1997).

Akiyama showed that interlaminar processes in human cortex expressed CD44 (Akiyama, Tooyama, Kawamata, Ikeda, and McGeer 1993). Korzhevskii described astrocytes that were located within layer I–not in the pia–that extended long, fine, unbranched processes running perpendicular through the cortical layers toward the white matter, and he called them *translaminar processes* (Korzhevskii, Otellin, & Grigor'ev, 2005). Korzhevskii did not clarify whether these translaminar processes were those previously described as interlaminar processes by Colombo. In 2014, Sosunov used the term *interlaminar* to refer to GFAP+/CD44+ processes that originated in layer I but not at the pia, and these processes were likely the same as those described by Korzhevskii (Sosunov et al., 2014). As a result, similar terminology has been used to identify the interlaminar processes emerging from two distinct astrocyte populations. While the interlaminar process originally described by Andriezen and depicted by Retzius, and probably most of those described by Colombo, originated from astrocytes whose soma was contacting the pia matter, Sosunov used the same term to identify processes originating from astrocytes located deeper in layer I, with somata not in contact with the pia, and that were referred to as translaminar processes by Korzhevskii. Cajal's drawings included both ILA somata located in layer I that contacted the pia, and ILA somata located deeper in layer I, with both cell types extending interlaminar processes.

Here, we performed a thorough analysis of GFAP+ astrocytes located in layer I that extended interlaminar processes and clarified the terminology of the two types of ILA: somata contacting versus not contacting the pia. We determined whether these cells were present in the cerebral cortex of 46 mammalian species, including 22 primates, and characterized and compared the principle features of ILA across species.

2 | MATERIALS AND METHODS

2.1 | Specimens

Species included in this study are shown in Figure 2. *Rattus norvegicus*, *Mus musculus, Microtus orchogaster, Mustela putorius, Monodelphis domestica, Ovis aries, Macaca mulatta, and Macaca fascucularis* brains were collected at UC Davis under previous approval of the UC Davis Institutional Animal Care and Use Committee. Microchiropteran bat samples were collected from the wild in Trinidad. Wild-caught specimens were collected, processed, and exported with the permission of the Wildlife Section, Forestry Division of the

Ministry of Agriculture, Land and Fisheries of the Republic of Trinidad and Tobago (Martínez-Cerdeño et al., 2017). Specimens of *Balaenoptera acutorostrata, Phocoena phocoena, Loxodonta africana,* all megachiropteran bat species, *Perodicticus potto*, *Papio ursinus,* and *Chlorocebus pygerythrus*, were collected from wild populations in Iceland, Greenland, Zimbabwe, the Democratic Republic of the Congo and Kenya, under appropriate local governmental approval of the relevant agencies in those countries.Specimens of *Hippopotamus amphibius, Tupaia belangeri, Lemur catta, Cebuella pygmaea* and *Saguinus imperator,* were obtained from the Copenhagen Zoo following euthanasia in line with management decisions of the zoo. These animals were treated and used according to the guidelines of the University of the Witwatersrand Animal Ethics Committee, which correspond to those of the NIH for care and use of animals and scientific experimentation. Postmortem brain specimens from additional species were acquired from Association of Zoos and Aquariums-accredited zoos or American Association for Accreditation of Laboratory Animal Care-accredited research institutions and maintained in accordance with each institution's animal care guidelines. Human samples were obtained from the Pathology Department at the University of California, Davis, Health System. Control tissue was obtained from subjects who did not have any significant neurological history. Human tissue specimens were obtained through consented autopsies with institutional review board approval.

2.2 | Tissue processing

All rodents, chiropterans, ferret, opossum, tree shrews, sheep, harbor porpoise, and some primates (*Macaca mulatta, Macaca fascicularis*), used in the current study were sacrificed and intracardially perfused with saline followed by with 4% paraformaldehyde (PFA) in 0.1 M Phosphate-buffered saline (PBS), (Dell et al., 2016a,2016b). The brains of *Hippopotamus amphibius* and *Loxodonta africana* were perfused immediately after death through the internal carotid arteries with saline followed by 4% PFA in PBS according to the protocol described by Manger et al. (2009) and Dell et al., (2016b). The brain of *Balaenoptera acutorostrata* was immersion-fixed in 4% PFA in 0.1 M PBS following extraction from the skull. The volume of both saline and PFA used during the perfusion process varied in relation with the size of the body or head of the animal (Charvet et al., 2017; Martínez-Cerdeño et al., 2016). For all the specimens listed above, the brains underwent postfixation by immersion in 4% PFA for 2–4 days at 4°C (depending on brain size), washed by 1X PBS, and cryo-protected in 30% sucrose in 0.1 M PBS at 4°C for at least 2 days. Tissue blocks of the species above were embedded into Killik OCT (#4585, Thermo-Fisher, Waltham, MA), frozen with 2-methylbutane, serially sectioned on a Leica cryostat at 16 μm and mounted on coated glass slides (#12–550-15, FisherScientific, part of ThermoFisher). The rest of the species included in this study, including human, were collected postmortem (postmortem interval < 24 hr for human, <14 hr for the rest of species) and immersion-fixed in 10% buffered formalin solution for at least 10 days. Specimens were transferred to a 0.1 M PBS containing 0.1% sodium azide at 4°C for storage prior to sectioning. Samples were cryoprotected in a graded series of 10, 20, and 30% sucrose solutions and cut frozen (Ariza et al., 2017; Hashemi, Ariza, Rogers, Noctor, & Martínez-Cerdeño, 2017). Tissue blocks of all species were sectioned (40 μm-thick sections, or 14 μm for human) perpendicular to the main axis of the gyrus contained in each block using a Leica SM2000R freezing sliding

microtome (Buffalo Grove, IL). Sections were placed into individual centrifuge tubes containing cryoprotectant solution (30% dH_2O, 30% ethylene glycol, 30% glycerol, 10% 0.244 M PBS), numbered sequentially, and stored at −20°C until histological or immunohistochemical processing. Antemortem observations for captive animals revealed no obvious neural deficits or behavioral abnormalities, and postmortem examination revealed no gross neuro-anatomical abnormalities.

2.3 | Immunostaining

One section from each sample was stained with cresyl violet (Nissl staining) for histological reference. Sections adjacent to the Nissl-stained section were used for immunostaining. For enzymatic immunohistochemistry staining, sections were first placed in blocking solution (10% donkey serum (ThermoFisher), 0.1% Triton X-100 (#9002–93-1, Millipore Sigma, Darmstadt, Germany) in TBS) for 1 hr at room temperature (RT). Sections were then incubated overnight at 4°C with the following primary antibody: GFAP (rabbit polyclonal 1:400, Z0334, former DAKO, now Agilent, Santa Clara, CA, RRID:AB_10013382), diluted in blocking solution. In the case of human samples, heat-mediated antigen retrieval was performed (110°C, for 8 min). Sections were washed with PBS and incubated with donkey antirabbit secondary antibodies that were conjugated with biotin (1:150, Jackson ImmunoResearch, West-Grove, PA, RRID:AB_2340593), amplified with avidin-biotin complex (ABC), and developed with DAB substrate (#SK-4105, Vector Laboratories, Burlingame, CA). All sections were dehydrated and coverslipped with Permount (#SP15–500, FisherScientific, part of ThermoFisher) and stored at RT.

For immunofluorescence staining, *Macaca mulatta* sections were blocked in blocking solution (10% donkey serum, 0.1% Triton X-100 in PBS) for 1 hr at RT, incubated overnight at 4°C with the following primary antibodies: APC (mouse monoclonal 1:300, #0P80, Millipore Sigma, RRID:AB_2057371), Aqp4 (rabbit polyclonal 1:400, #, AB3594, Millipore Sigma, RRID:AB_91530), GFAP (rabbit polyclonal 1:400, Z0334, former DAKO, now Agilent, RRID:AB_10013382), GFAP (mouse monoclonal 1:400, G3893, Millipore Sigma, RRID:AB_477010), Iba1 (rabbit polyclonal 1:400, #019–19,741, FUJIFILM Wako Pure Chemical Corporation, Richmond, VA, RRID:AB_839504), Ki67 (rabbit polyclonal 1:400, ab15580, Abcam, Cambridge, MA, RRID: AB_443209), MAP2 (rabbit polyclonal 1: 400, ab32454, Abcam, RRID: AB_776174), NeuN (mouse monoclonal 1:100, MAB377, Millipore Sigma, RRID:AB_2298772), Olig2 (rabbit polyclonal 1:100, #AB9610, Millipore Sigma, RRID:AB_570666), S100b (rabbit polyclonal 1:300, ab52642, Abcam, RRID:AB_882426), Sox10 (rabbit polyclonal 1:300, ab27655, Abcam, RRID:AB_778021). Sections were rinsed with PBS and incubated for 1 hr at RT with AlexaFluor#488 or AlexaFluor#594 conjugated polyclonal antirabbit/mouse antibodies (1:600, Jackson ImmunoResearch, RRID:AB_141708, RRID:AB_141633) and DAPI (1:1000, #10236276001, Hoffmann-La Roche, Basel, Switzerland) to label nuclei. In the immunostaining for blood vessels, tissues were incubated overnight at 4°C with a biotin conjugated Lectin (1:200, L2140, Millipore Sigma, Darmstadt, Germany, RRID:AB_2313663), and then incubated with Alexa#594-conjugated Streptavidin (1:500, S11227, Invitrogen, part of ThermoFisher, RRID:AB_2313574). The primary antibody was omitted as negative control for each experiment. All antibodies and DAPI were diluted in

blocking solution. Slides were cover-slipped with Mowiol (#81381, Millipore Sigma) and stored at4°C.

2.4 | Antibody characterization

Anti- APC (Ab-7): *Immunogen:* a recombinant protein consisting of amino acids 1–226 of APC; *Host:* Mouse: *Isotype:* IgG2b; *Antibody type:* monoclonal, clone CC-1; *Manufacturer and Catalogue#*: Millipore Sigma, #OP80; *Concentration:* 1:300; *Characterization reference:* immunohistochemistry on rat spinal cord (McTigue, Wei, & Stokes, 2001); *Additional information:* It recognizes APC in oligodendrocytes and astrocytes. RRID:AB_2057371.

AntiAqp4: *Immunogen:* GST fusion protein with residues 249–323 of rat Aquaporin 4 (SwissProt accession number P47863). It is expected that the antibody may also react with mouse (73/75), bovine (71/75), human (69/75), and rabbit (64/75) due to sequence homology; *Epitope:* C-terminus; *Host:* rabbit; *Antibody type:* polyclonal; *Manufacturer and Catalogue#:* MilliporeSigma #AB3594; *Concentration:* 1:400; *Characterization reference:* WB in rat brain lysate, band size 34 kDa (Zeng et al., 2010); *Additional information:* It recognizes the water-specific channel Aquaporin 4, located in the gastrointestinal tract, kidney and brain. In CNS tissue, AntiAQP4 usually labels astrocyte endfeet. RRID:AB_91530.

AntiGFAP (rabbit): *Immunogen:* GFAP isolated from cow spinal cord; *Host:* rabbit; *Antibody type:* polyclonal; *Manufacturer and Catalogue#:* Agilent #Z0334; *Concentration:* 1:400; *Characterization reference:* WB in postmortem human samples, frontal cortex (Garcia-Esparcia et al., 2018); *Additional information:* This antibody works with several species. The protein GFAP shows 90–95% homology between species (Rutka et al., 1997), and as demonstrated by immunohistochemistry, the antibody cross-reacts with GFAP in cat, dog (Boya & Calvo, 1993), mouse, rat (Castellano et al., 1991), and sheep (Hansen, Stagaard, & Møllgård, 1989). Additionally, it reacts strongly with human and cow GFAP. RRID:AB_10013382.

AntiGFAP (mouse): *Immunogen:* GFAP from pig spinal cord; *Host:* mouse; *Antibody type:* monoclonal; *Manufacturer and Catalogue#:* MilliporeSigma G3893; *Concentration:* 1:400; *Characterization reference:* WB in Hela cells transfected with human full-length GFAP construct, Knock-in mice (GFAPR236H/+) heterozygous for the R236H mutation and transgenic mice (GFAPTg) overexpressing human wild-type GFAP, band size 5 kDa (Lin, Messing, & Perng, 2017); *Additional information:* The antibody reacts specifically with GFAP in immunoblotting assays and labels astrocytes, Bergmann glia cells and chondrocytes of elastic cartilage in immunohistochemical staining. RRID:AB_477010.

AntiIba1: *Immunogen:* Synthetic peptide corresponding to C-terminus of Iba1; *Host:* rabbit; *Antibody type:* polyclonal; *Manufacturer and Catalogue#:* WAKO #019–19,741; *Concentration:* 1:400; *Characterization reference:* WB in Iba1-expressing Swiss 3 T3 cells, band size 17 kDa (Kanazawa, Ohsawa, Sasaki, Kohsaka, & Imai, 2002); *Additional information:* This antibody reacts with Iba1 protein expressed in macrophage/microglia. RRID:AB_839504.

AntiKi67: *Immunogen:* Synthetic peptide conjugated to KLH derived from within residues 1,200–1,300 of Human Ki67; Peptide available as Abcam # ab15581; *Host:* rabbit; *Antibody type:* polyclonal; *Manufacturer and Catalogue#:* Abcam ab15580.

Concentration: 1:400; *Characterization reference:* immunofluorescence in mouse renal cortex (Loganathan et al., 2018). RRID: AB_443209.

AntiMap2: *Immunogen:* Synthetic peptide conjugated to KLH derived from within residues 1–100 of Rat MAP2. Peptide available as Abcam #ab32453; *Host:* rabbit; *Antibody type:* polyclonal; *Manufacturer and Catalogue#:* Abcam ab32454; *Concentration:* 1: 400; *Characterization reference:* WB in mouse brain lysates, band size 280 kDa (Li, Li, Gao, & Yang, 2018). RRID:AB_776174.

AntiNeuN (A60): *Immunogen:* Purified cell nuclei from mouse brain; *Host:* mouse; *Antibody type:* monoclonal, clone A60; *Manufacturer and Catalogue#:* MilliporeSigma MAB377; *Concentration:* 1:100; *Characterization reference:* IF staining on mouse hippocampal slice (Krzisch et al., 2015); *Additional information:* This antibody reacts with most neuronal cell types throughout the nervous system of mice including cerebellum, cerebral cortex, hippocampus, thalamus, spinal cord, and neurons in the peripheral nervous system including dorsal root ganglia, sympathetic chain ganglia, and enteric ganglia. The immunohistochemical staining is mainly localized in the nucleus of the neurons with lighter staining in the cytoplasm. The cell types that do not react with MAB377 include Purkinje, mitral, and photoreceptor cells. RRID:AB_2298772.

AntiOlig2: *Immunogen:* Recombinant mouse Olig-2; *Host:* rabbit; *Antibody type:* polyclonal; *Manufacturer and Catalogue#:* MilliporeSigma #AB9610; *Concentration:* 1:100; *Characterization reference:* Immunofluorescence on E9.5 mouse embryos (Makino et al., 2015); *Additional information:* It reacts with oligodendrocytes in the central nervous system, in oligodendrogliomas, in glioblastoma, and moderately in astrocytomas. RRID:AB_570666.

AntiS100 β: *Immunogen:* Synthetic peptide within Human S100 beta aa 50 to the C-terminus (C terminal). The exact sequence is proprietary; *Host:* rabbit; *Antibody type:* monoclonal, clone (EP1576Y); *Manufacturer and Catalogue#:* Abcam ab52642; *Concentration:* 1:300; *Characterization reference:* WB astrocytes cell culture, band size 11 kDa (Du et al., 2018). RRID:AB_882426.

AntiSox10: *Immunogen:* Synthetic peptide: CPPAHSPTANWDQP-VYTTLT, corresponding to C-terminal amino acids 449–468 of Chicken SOX8; *Host:* rabbit; *Antibody type:* polyclonal; *Manufacturer and Catalogue#:* Abcam ab27655; *Concentration:* 1:300; *Characterization reference:* WB in human embryonic stem cells lysate, band size 50 kDa (Werner et al., 2015). *Additional information:* It reacts with Sox10 protein expressed in fetal brain and in adult brain oligodendroglial cells in mouse (Chen et al., 2016), neural crest in mouse (Dai et al., 2013; Mukhopadhyay, Jarrett, Chlon, & Kessler, 2009) and chicken (Sasai, Kutejova, & Briscoe, 2014), Schwann cells in human and rat (Chen et al., 2016), and small intestine in human (Pelletier et al., 2017). It localizes in the cytoplasm and/or in the nucleus. RRID:AB_778021.

2.5 | Imaging

In the case of enzymatic immunohistochemistry, brightfield pictures were taken on an Olympus microscope (Olympus corporation, Tokyo, Japan), equipped with a high-resolution camera, using a 40x oil objective. Brightfield images were taken as Z-stacks of an average of ten 1.8 mm-spaced focal planes and merged with the StackFocuser plugin of Fiji software. For immunofluorescence, pictures were taken with a Nikon C2 or a Nikon A1 confocal microscope (Nikon, Melville, NY), as Z-stacks of at least ten 1.8 μm-spaced focal planes and merged in MAX-modality on Fiji software (RRID:SCR_002285). 60x oil and 100x oil objectives were used.

2.6 | Quantification

For linear density analysis, we counted the number of pial ILA and rudimentary ILA in contact with the pia matter. We defined the density value as the number of ILA per the pial length (mm). ILA density was measured in three 5 mm wide images per specimen.

2.7 | Neurolucida analysis

At least five ILA were randomly selected from ventral and from dorsal frontal cortex of each species. Pial ILA were identified by the soma being attached to the pial surface, and by processes extending toward the deeper layers of the cortex. Cells were chosen based on a presence of GFAP immunostaining and no staining artifacts. Each cell was scanned under a 40x oil objective by varying the depth of the Z plane with Neurolucida 8 software MBF Bioscience, Willinston, VT (RRID: SCR_001775) and an Olympus microscope equipped with a highresolution digital camera, a mechanical stage and an x-y-z axis encoder. The following parameters were analyzed: number of primary processes, number of total processes (branching nodes), total length of the processes, and complexity index (Complexity = [Sum of the terminal orders + Number of terminals] * [Total dendritic length/ Number of primary dendrites]). Two-images of the 3D reconstructions were generated and are shown in Figures 7–9.

2.8 | Statistical analysis

In Figure 6a,b, Figure 7b–e, and Figure 8b–e, data from each species belonging to the same order or suborder was averaged, and standard deviations and standard errors calculated for each order. In Figure 8f–i and Figure 9e–t, data obtained from single cells of the same species was averaged, and standard deviations and standard errors calculated for each species. Results were compared among different species/orders using α *t*-test. Statistical significance was set at an α level of 0.05. When there was only one species within an order, standard values were not calculated.

3 | RESULTS

3.1 | Two types of ILA: Pial and subpial

We investigated frontal cerebral cortex from 46 mammalian species, representing almost all orders of therian mammals (Figure 2, Table 1). We first analyzed the cerebral cortex of *Macaca mulatta,* which has been shown to possess interlaminar processes (Colombo et al.,

2000), and for which we have an ample collection of tissue. We observed GFAP$^+$ long processes that coursed from layer I through the cortical laminae to end in the supragranular layers and, in some cases, in layer IV. We identified the origin of these processes in thin sections and traced them to two distinct types of GFAP$^+$ somata. Most interlaminar processes (~95–98%) originated from somata that were in contact with the pia and that exhibited the morphology of ILA as originally described by 19th century neuroanatomists. The remaining GFAP$^+$ processes originated from multipolar cells that were located in upper layer I. Based on the cellular origin of the interlaminar processes, we determined that the processes originating from cell somata contacting the pia are those that were described by Andriezen (1893), while the processes emerging from cells in layer I that did not contact the pia are those described by Korzhevskii (2005). As both cell types have been referred to as ILA, and both extend interlaminar processes that course toward layer IV, we maintain the term ILA; however, as these cells differ in soma morphology and location, we use the terms *pial* (Figure 3a) and *subpial* (Figure 3c), to distinguish these two distinct cell types (Figure 3).

We found that the morphology of pial ILA varied between species. In macaque and most other primates studied, the pial ILA possessed a soma that had an inverted pyramidal morphology with the base contacting the pia. Several processes, usually 4–5, originated from the apex of the pyramid and a smaller number originated from other portions of the soma. The proximal portion of the ILA processes was thicker, and the distal portion became progressively thinner as it coursed through the depth of the cortex. Most processes terminated in layers II and III, and a minority reached the upper portion of layer IV. Most pial ILA extended 1–2 interlaminar processes. We did not observe the superficial tangential system of fibers that formed a true felt-work, nor the few shorter fibers passing to the superjacent pia, as originally described by Andriezen (1893). In contrast, somata of subpial ILA were round/oval and primarily located in the upper portion of layer I. They possessed multiple processes (5–15) that can be classified as one of three types. The first type of processes that emerge from subpial ILA soma showed no specific orientation and remained within layer I. These type 1 processes are the most numerous, and subpial ILA extend 3 to 10 of these processes. The second type of processes was short and initially extended superficially to contact the pia. Subpial ILA possess 1–3 of these type 2 processes. The third type of processes was the interlaminar process that descend towards layer IV. Subpial ILA possessed 1–2 interlaminar, or type 3, processes. The interlaminar processes primarily coursed perpendicular to the pia, although in some cases the processes descended at an oblique angle. In primate species, we observed interlaminar processes that crossed paths with other interlaminar processes. The trajectory of the interlaminar processes varied from those with a perfectly straight path (e.g., Figure 4m,r), to those with a “wavy” trajectory (e.g., Figure 4h,u). Some processes curved sharply and nearly completed a full circumference (Figure 4v). We observed that in most species some of the interlaminar processes ended in varicosity-like enlargements or bulbs (Figure 4w), as previously reported (Colombo, Gayol, et al., 1997; Colombo et al., 1998; Colombo, Reisin, Miguel-Hidalgo, & Rajkowska, 2006; Colombo, Schleicher, & Zilles, 1999; Oberheim et al., 2009; Oberheim, Wang, Goldman, & Nedergaard, 2006). These bulbous endings were previously described to

contain electron-lucent material and mitochondria under electron microscopy inspection of nonhuman primates and human cerebral cortex (Colombo, Gayol, et al., 1997).

3.2 | All therian mammals investigated present typical, or rudimentary, ILA

We first examined radial processes in the dorsal cortex and found that the length of the processes varied among species. In some species, processes projected toward deep layers but were very short and did not exit layer I, however, we were able to identify them based on their emergence from an inverted pyramidal-shaped soma that was in contact with the pia. We refer to these astrocytes with short processes as *rudimentary pial ILA,* to distinguish them from pial ILA with interlaminar processes that exited layer I and coursed through the cortical lamina, which we refer to as *typical pial ILA.* We hypothesize that rudimentary ILA evolved into typical ILA across mammals. We also found *rudimentary subpial ILA* with processes that remained within layer I, and *typical subpial ILA* with processes that exited layer I.

Included among the mammalian species that possessed rudimentary pial ILA were species of Marsupialia included in our analysis and species belonging to the orders Xenarthra and Rodentia. The remaining mammalian species (Primate, Scandentia, Chiroptera, Carnivora, Artiodactyla, Hyracoidea, and Proboscidea) exhibited typical interlaminar processes that exited layer I. Some species had pial ILA that were only present in the ventral cortex, while other species had pial ILA in both ventral and dorsal cortices. Rudimentary pial ILA had fewer, shorter, and less complex processes (see Figures 3 and 4).

Subpial ILAs were absent in marsupials but rudimentary forms of the subpial ILAs were present in the ventral cortex of most mammalian orders analyzed (Xenarthra, Hyracoidea, Proboscidea, Rodentia, Scandentia, Carnivora, Artiodactyla). We only observed rudimentary subpial ILA in the dorsal cortex of Xenarthra, Hyracoidea, Scandentia, and Carnivora. Typical subpial ILA were only present in primates, and in particular, anthropoid species (i.e., New World monkeys, Old World monkeys, and apes).

A list of species containing rudimentary and typical pial ILA and subpial ILA in dorsal and ventral cortices is found in Table 1. Herein, we will focus on pial ILAs, with more details on subpial ILA to be provided in a follow up study.

3.3 | Molecular characterization of ILA

To further verify the astrocytic nature of pial ILA, we performed colocalization studies of the $GFAP^+$ ILA using other neural makers in cortical tissue from rhesus monkeys (*Macaca mulatta*). We determined that $GFAP^+$ ILA in rhesus monkeys also expressed the glial markers vimentin and APC, the astroglial markers S100β and AQP4, but did not express the oligodendrocyte markers OLIG2 or S0X10, neither the neuronal markers NeuN or MAP2, nor the microglial marker Iba1. This expression pattern agrees with the astrocyte phenotype of ILA (Figure 5).

3.4 | The density of ILA varies slightly among mammalian species

The linear density (number of ILA somata per mm of pia) varied slightly among mammalian species (Table 2, Figure 6). There was a twofold difference between the mammalian orders with the highest and lowest density of ILA. Species with lowest density of ILA were Marsupialia (15.6 ± 4.2 ILA/mm) and Scandentia (15.4 ILA/mm), while the order with the highest density was Primates (32.7 ± 1.6 ILA/mm), followed by Proboscidea (25.1 ILA/mm).

Among primates, Old World monkeys, great apes and humans had the highest linear density of ILA (34.1 ± 2.8; 37.9 ± 2.3; and 37.0 ILA/mm, respectively). Strepsirrhines, tarsiiforms, and New World monkeys presented with a slightly lower density of ILA (29.1 ± 5.4; 23.8; and 27. 3 ± 2.4 ILA/mm). Among great apes, bonobos and chimpanzees (*Pan paniscus* and *Pan troglodytes*) had the highest density of ILA among all mammalian species (44.4 and 41.6 ILA/mm, respectively). Primates with the lowest density of ILA were strepsirrhine (i.e., loris and lemur) species (*Perodicticus potto* and *Lemur catta*; 24.5 and 23.0 ILA/mm, respectively). The remaining orders presented with a similar linear density of ILA. Rodents: 22.4 ± 1.2, Carnivores: 17.4 ± 1.2, and Artiodactyls: 17.3 ± 1.5. Among Artiodactyls, cetaceans had a slightly increased ILA density (19.1 ± 1.2 ILA/mm). All species of microchiropterans and megachiropterans (bats) presented similar average density of ILA: 18.7 ± 1.5 ILA/mm (Table 2, Figure 6).

3.5 | The complexity of ILA greatly varies among mammalian species

We stained cortical tissue with antibodies against GFAP and reconstructed at least five ILA from each species using Neurolucida. We obtained data for the number of primary processes, the total number of processes, the sum of the length of all processes per ILA, and the complexity of ILA (Table 2, Figures 7–9, see methods).

We found that, among mammalian orders, the number of primary processes varied twofold, the total number of processes varied fourfold, the length of processes varied more than fivefold, and the complexity value varied by a factor of 17. Marsupials had the lowest average number of primary processes (1.5 ± 0.13 per ILA), while primates and bats had the highest average number of primary processes (primates: 3.6 ± 0.2; bats: 3.1 ± 0.5). Among primates, strepsirrhines had the fewest primary processes with 2.2 ± 0.1 per ILA, and human had the highest number of primary processes at 5.1 per ILA, closely followed by New World monkeys (4.5 ± 0.6). Conversely, Old World monkeys and great apes ILA possessed fewer primary processes (3.3 ± 0.4 and 3.6 ± 0.3, respectively). Among primates, species with the most primary processes were the New World monkeys *Pithecia pithecia, Cebuella pygmaea,* and *Saguinus imperator* (5.4, 4.4, 5.3), the Old World monkey *Papio ursinus* (5.3), and the great apes *Gorilla gorilla* (4.7) and human (5.1). The species with the fewest primary processes was the lemur *Cheirogaleus medius* (1.7). Rodents had an average of 2.2 ± 0.4, carnivores 2.2 ± 0.4, and artiodactyls 2.0 ± 0.1 primary processes. Among bats, the megachiropteran *Epomops franqueti* presented the most numerous primary processes (5.0), while remaining bats had a similar number of primary processes (2.3–3.0, Table 2, Figures 7 and 9).

We next analyzed the total number of processes emerging from ILA. The total number of processes was lowest in Hyracoidea, Proboscidea, and Marsupialia (4.4, 4.8, 4.9 ± 0.6, respectively), and highest in Primate (16.3 ± 1.4). Among primates, strepsirrhines had the lowest total number of processes (6.7 ± 0.4), while great apes (excluding human) and human (23.7 ± 0.9, and 27.9, respectively) were the groups with the most abundant total number of processes. The primates with the lowest number of processes were *Cheirogaleus medius* and *Lemur catta* with 5.7 and 6.7, respectively. The species with the highest number of processes were bonobo (*Pan troglodytes*) and human (26.9 ± 5.1 and 27.9 processes per ILA, respectively). The remaining orders presented a similar number of total processes. Rodents had 7.1 ± 0.8, carnivores 6.5 ± 0.8, artiodactyls with 6.7 ± 0.7, and bats with 6.7 ± 1.1 total number of processes per ILA.

The sum of the length of all processes per ILA was shortest in marsupials (79.4 ± 4.6 μm) and longest in primates (379.3 ± 37.9 μm). Among primates, strepsirrhines had the lowest process length (157.9 ± 19.8 μm), while the longest were found in the New World *Pithecia pithecia* (445.5 μm), the Old World *Cercocebus agilis* (540 μm), and the great apes *Pan paniscus* (713.5 μm), *Pan troglodytes* (720 μm), *Pongo pygmaeus* (593.9), and human (593.4 ± 31.0 μm). The remaining species presented a similar total process length. Rodents: 118.2 ± 8.8 μm; carnivores: 137.4 ± 17.0 μm, artiodactyls: 166.6 ± 29.8 μm, and chiropterans: 124.8 ± 28.4 μm.

We next quantified the complexity of ILA. The complexity index accounts for the number of primary processes, the total number of processes, and the total length of processes, as described in (Pillai et al., 2012). The complexity of ILA processes was very similar across mammalian species, with the exception of bats where complexity was slightly lower (725.5 ± 196.4 complexity units), and for primates for whom it was greatly increased when compared to all other orders represented in our analysis (12,355.4 ± 2,514.0 units). The lowest ILA complexity among primates was found in the lemurs *Cheirogaleus medius* and *Lemur catta,* and the loris *Perodicticus potto* (1,425.6, 2,009.5, and 1,793.7, respectively). Primates with the highest ILA complexity were bonobo, chimpanzee, orangutan, and human (44,416.5; 32,019.6; 28,101.8; 25,221 ± 4,765; respectively). The remaining orders presented similar complexity values (rodents: 1,317.8 ± 146.2; carnivores: 1,500.5 ± 77.6; artiodactyls: 2,717.8 ± 875.4). Among all mammalian orders, primate ILA had the highest complexity values, and within primates, great apes and human displayed extremely complex ILA. These data indicate that the complexity of ILA processes has evolved differently among species.

3.6 | ILA contact capillaries and neuronal processes

We investigated the possibility that ILA were proliferative cells by staining rhesus macaque cortical tissue with the proliferative marker Ki67 and did not find colocalization of GFAP and Ki67, suggesting the nonproliferative nature of ILA (n = 100 cells, Figure 10a). We next investigated whether there are potential contacts between interlaminar processes and other cortical components. We found that $MAP2^+$ neuronal processes contacted $GFAP^+$ ILA processes, suggesting astrocyte-neuron interactions (Figure 10b). We also examined colocalization of $GFAP^+$ ILA and with the capillary marker lectin and found that

interlaminar processes originating from ILA somata contacted the walls of capillaries. We analyzed confocal Z-stack images and found that ILA processes contacted and sharply curled around the perimeter of capillaries (Figure 10c,d). These points of contact between ILA and capillaries likely correspond to the sharp curves we observed in some ILA processes.

4 | DISCUSSION

4.1 | Two types of ILA: Pial and subpial

We analyzed $GFAP^+$ cells in layer I of the therian mammal cerebral cortex that give rise to previously described interlaminar processes (Andriezen, 1893; Colombo et al., 1995). Analysis in thin-cut sections allowed us to trace interlaminar processes to the cell of origin and observe the morphological phenotype of these cells. We concluded that there are two subtypes of ILA that share basic features: both cell types are astrocytes that extend interlaminar process and have a soma positioned within layer I. However, these cells have distinct morphologies and soma locations within layer I, and their presence in the cerebral cortex varies across mammalian species. To distinguish among these distinct cell types, we termed them *pial ILA and subpial ILA* (Table 1). Pial ILA have an inverted pyramidal shape with the base of the soma contacting the pia (Andriezen, 1893). In contrast, subpial ILA are multipolar cells with a round or oval soma that is located in the lower upper layer I and the soma does not contact the pia. We were able to confirm the presence of typical pial ILA and rudimentary pial ILA in all mammalian species included for analysis, while subpial ILA were not present in all species and typical subpial ILA were only present in certain primate species. In macaque, the processes of pial and subpial ILA intermingle and can only be distinguished by tracing the processes to the soma of origin. Rhesus monkeys are one of the species in our analysis that had more subpial ILA, accounting for 2–5% of total processes. These data suggest that pial ILA are substantially more abundant than subpial ILA. Here we discuss the properties of pial ILA and will focus on the nature of subpial ILA in future studies.

4.2 | Pial ILA express astrocyte markers

In the early Golgi impregnation studies, ILA were categorized as astrocytes based on their morphology. The astrocytic phenotype was later confirmed by GFAP expression and the lack of MAP2 expression (Colombo et al., 1998). We further investigated the molecular expression properties of ILA in macaque cortical tissue and confirmed that ILA also express the glial markers vimentin and APC, the astrocyte markers S100β and AQP4, but do not express neuronal, oligodendroglial, or microglial markers. This pattern of marker expression corroborates the already known astrocytic nature of ILA.

4.3 | Pial ILA distribution

The distinct morphology of pial ILA somata allowed us to identify what we term a rudimentary form of ILA. We defined rudimentary ILA and typical ILA based on the length of their processes. Both cell types had inverted pyramidal cells with the base contacting the pia, but typical ILA possessed interlaminar processes that exited layer I, while rudimentary ILA possessed at least one process that coursed towards layer II but did not exit layer I.

It was previously described that in addition to primates, some megachiropteran species and tree shrews, evinced interlaminar processes in the ventral cortex (Colombo et al., 2000), and we confirm this observation. In addition, we found that while Marsupialia and the Eutherian orders Rodentia and Eulipotyphla only possessed rudimentary pial ILA, the remaining mammalian species in our analysis (orders Xenarthra, Primates, Scandentia, Chiroptera, Carnivora, Artiodactyla, Hyracoidea, and Proboscidea) possessed pial interlaminar processes that exited layer I. However, while most species possessed ILA positioned along the entire cortical pial surface (dorsal and ventral), in some species ILA were only present in the ventral cortex, most often at the level of the neopaleo cortical junction. Species that had pial ILA only in ventral cortex included marsupial species, hedgehog (*Atelerix frontalis*), and hippopotamus (*Hippopotamus amphibius*). These were ventral rudimentary ILA. Harbor porpoise (*Phocoena phocoena*) had ventral rudimentary ILA and dorsal ILA with longer interlaminar processes that exited layer I. Among other species that had pial ILA in the dorsal cortex, only Primates, Hyracoidea (hyrax), and Proboscidea (elephant) possessed typical ILA. The distinct pattern of pial ILA distribution across species that are only distantly related to each other may suggest that during the course of mammalian evolution, pial ILA evolved in the neocortex of some species but not others. In those species that presented pial ILA in both ventral and dorsal cortex, the linear density of ILA along the pial surface in coronal sections was often similar or slighter higher in the ventral cortex. However, we noted that the linear density of ILA varied among species, being twofold higher in primates (the order with the highest density)–than in tree shrews (the order with the lowest density). These data suggest that the linear density of ILA changes mildly across phylogeny. Although it is notable that the most striking variation occurs between primates and their closest living relatives in our analysis, tree shrews.

4.4 | Pial ILA are the most complex in primates

We measured several morphological features of pial ILA. We found that the number of primary processes was similar in species from most orders that we analyzed, but there were species differences. For example, the number of primary processes was 2.5-fold higher in primates than in marsupials. Within primates, strepsirrhines had the fewest and human had the highest number of primary processes. The total number of processes and the number of primary processes followed a similar pattern across mammals, with the exception of primates for which these parameters were not entirely related. For example, New World monkeys possessed more primary processes than Old World monkeys and great apes but had a lower total number of processes. However, human cortex had more primary and more total processes.

The total number of processes was correlated with the total length of processes. We observed the lowest number of processes in marsupials and 4–5 fold more processes and 4–5 times greater length of processes in primates. Among primates, the total number of processes and total length of processes were generally lower in strepsirrhines species and higher in great apes and human. These measures gradually increased from strepsirrhines to New and Old World monkeys, and to apes including human. The parameter that varied the most among species was ILA complexity. The less complex ILA were present in marsupial and bats, while the most complex ILA were found in primates, with a 17-fold difference in complexity

values between these two extremes. Among primates the most complex ILA were observed in chimpanzee and bonobo, closely followed by orangutan and human. The remaining mammalian species presented an intermediate value of ILA complexity. Outside of primates, the species with the highest ILA complexity value was the minke whale (*Balaenoptera acutorostrata*). Since the other cetacean species analyzed, the harbor porpoise (*Phocoena phocoena*) showed fourfold less ILA complexity, we reasoned that perhaps body size was related to ILA complexity (minke whale: 4–5 tons, porpoise: 60–75 kg). However, other large species such elephant (3–4 tons) possessed ILA with the same complexity as the harbor porpoise, while sheep (*Ovis aries*) had a complexity value similar to that of whale. Among rodents, ILA complexity was threefold higher in the vole than in laboratory rat and mouse. Whether wild rat or mouse would have a higher ILA complexity than laboratory animals, similar to that of vole, is an important point that should be investigated. Other than whale, sheep, and vole, the remaining nonprimate species included for analysis presented similar complexity values. We did not observe a correlation between the length of processes and the thickness of the cortex. However, further studies will be needed to address this point.

4.5 | Rudimentary ILA may develop into typical ILA across mammalian evolution

Our results suggest that radial processes originating in layer I and projecting toward deep layers are a shared characteristic among therian mammals, including marsupials. According to our observations, during evolution, these processes that originate from rudimentary ILA and are present in the cortex of more ancient mammals, may have become more complex and extended their length beyond the limit of layer I, as it is observed in typical ILA in the lateral cortex of bats, carnivores, and cetaceans, and then in the dorsal cortex as in primates, hyrax, and elephant. Once these processes became interlaminar, they continued evolving by increasing their morphological complexity. Consistent with this idea, among primates, strepsirrhines exhibited the least complex ILA while great apes possessed the most complex ILA, indicating an evolutionary process of increasing ILA complexity within primates.

4.6 | Technical considerations

Some technical issues should be considered to properly interpret these data. While brain tissue from most species in our study were transcardially perfused with fixative, this was not the case for all species, such as human, many of the primates, and whale. The postmortem interval (PMI), the time between death and the time of brain fixation, also varied among cases. This should be considered when comparing data across species (e.g., the complexity and related values measured of ILA in human and other great apes). Among great apes, bonobo, chimpanzee, and orangutan, presented slightly higher ILA complexity than human. This may reflect actual morphological differences between species. On other hand, the data may be influenced by the state of preservation of human tissue. We also need to consider that, for all the species except for human, we only analyzed tissue samples obtained from one individual. Thus, it is possible that the case examined was not representative of the average data that could be obtained from a larger sample in each species, as we did for example for human. We should also account for the extent of the brain analyzed. In small brains, as in mouse, a single slice encompassed both ventral and dorsal cortex and the whole expansion of the cortex was analyzed at once. In bigger brains like those of human or whale, we were only able to analyze smaller portions of the brain.

In some cases, our results were not in agreement with previously published findings, including which species possess ILA as proposed by Colombo and colleagues. The difference in conclusions may have resulted from different approaches in data analysis. For example, Colombo et al. focused their analysis on interlaminar processes, while we focused our study on the astrocyte soma from which radial process projecting to lower cortical layers are originated. Colombo also described short process in some species, for example short processes crossing lamina I and barely entering layer II in the dog (Colombo et al., 2000). While these processes in dog are not interlaminar, we would consider them as processes arising from rudimentary ILA. We included analysis of the rudimentary ILA subtype and their characteristics as this potentially reveals information about their evolutionary origin. However, other potential differences may not arise from the approach or focus of the study. Colombo et al. reported that Chiroptera, Insectivora, and Scandentia were the only species that presented interlaminar processes in the ventral cortex. In some cases, this may be explained because he did not examine the same species that we included in our study, for example, hyrax, elephant, cetaceans, and xenarthans. We also found ILA with interlaminar process exiting layer I in the ventral cortex of carnivores. However, we studied different carnivore species, while Colombo's team studied dog, we analyzed cat, tiger, ferret, and red panda. So, it is possible there are meaningful differences in ILA presence or characteristics among carnivores.

This project included 46 species. Tissue from some of these cases were cut in our laboratory at 14–16 μm, and others were received as already cut as 40-μm thick sections. The difference in section thickness could affect the obtained values, especially for ILA linear density. To deal with this problem, we analyzed materials in montages of 40x images that were produced from projections of Z-stacks that summarized 16–18 μm of the tissue thickness across all cases. In this manner, we compared images obtained from a similar thickness in a range of 14–18 μm across species. The difference of 4 μm could account for some differences in the data reported, but we believe that this variation is minor.

4.7 | Potential functions of ILA

ILA may share many functions with other astrocytes in the brain and in the cerebral cortex. As cortical protoplasmic astrocytes, ILA may participate in a wide variety of functions, including neurotransmitter reuptake and release, water distribution, pyruvate metabolism, reactive oxygen species removal, antioxidant metabolism, blood brain barrier regulation, ion buffering, the synthesis and secretion of trophic factors, among others (Schitine, Nogaroli, Costa, & Hedin-Pereira, 2015; Scuderi, Stecca, Iacomino, & Steardo, 2013; Sofroniew & Vinters, 2010). Sosunov and colleagues recorded from several long-process astrocytes in the human excised temporal lobes and found that they displayed passive electrophysiological properties similar to those of protoplasmic astrocytes. They also found no significant differences in resting membrane potential, input resistance, and membrane capacitance (Sosunov et al., 2014). However, ILA differ significantly from protoplasmic astrocytes in morphology. Protoplasmic astrocyte processes cover a spherical area of ~35–75 μm of cortical tissue within a single layer and the processes of one astrocyte intermingle with processes from neighboring astrocytes (Vasile, Dossi, & Rouach, 2017). In contrast, typical ILA have a long interlaminar process that cover a single mini-columnar area that spans

several layers. In other words, they cover a vertical, rather than spherical area, in which they could potentially interact with protoplasmic astrocytes, neurons, and other cortical structures throughout many layers of the cortex. Therefore, while ILA may share functions with protoplasmic astrocytes, they are unique in the fact that they might manage distant territories. Accordingly, Colombo proposed that interlaminar processes may represent long-range structures responsible for radially-organized glial-mediated influences on the ionic microenvironment in the cortex (Colombo et al., 1998). However, Sosunov et al. tested a potential participation of ILA in ion regulation by looking for contacts of interlaminar processes with nodes of Ranvier, known to participate in ion regulation (Lundgaard et al., 2013). They used Caspr1 as a paranodal junction marker but did not find any contact between nodes and $CD44^+$ long processes, while protoplasmic astrocytes did reveal contacts (Sosunov et al., 2014). The radial morphology of I LA processes may also be involved in maintaining columnar organization and function in the cortex (Colombo & Reisin, 2004). Consequently, species with more organized columnar structure present a greater number of longer interlaminar processes, as is the case with great apes.

We observed several interaction modalities of ILA with cortical structures. We described interlaminar processes in close proximity with both $MAP2^+$ neuronal neuropil and capillaries. A potential interaction between interlaminar processes and $MAP2^+$ neuropil would suggest an interaction between ILA and neurons. Furthermore, as reported before (Colombo, Gayol, et al., 1997; Sosunov et al., 2014), we detected a very close interaction between interlaminar astrocytes and capillaries. In some cases, we observed interlaminar processes that wrapped around the perimeter of capillaries. Accordingly, the water channel AQP4 known to be present in astrocytes in direct contact with blood vessels (Hubbard, Hsu, Seldin, & Binder, 2015), is expressed by ILA. These results suggest that ILA function as a component of the blood–brain barrier (BBB) in the upper layers of the cortex and may be involved in the maintenance of blood–brain barrier endothelial cell properties and regulation of blood–brain barrier permeability. Additionally, the expression of AQP4 by ILAs suggests a potential role for ILAs in the glymphatic system. This system involves the para-arterial influx of cerebrospinal fluid (CSF) into brain parenchyma, and a concomitant clearance of waste extracellular solutes, which are transferred from the interstitium to the CSF. AQP4-mediated astrocytic water transport has been shown to play an essential role in this pathway, which is specifically regulated during sleep (Aspelund et al., 2015; Bacyinski, Xu, Wang, & Hu, 2017; Iliff et al., 2012; Louveau et al., 2015).

In addition to morphology, ILA are different from cortical proto-plasmic astrocytes in their contact with the pia and expression of vimentin. Overall, ILA may mediate the communication of protoplasmic astrocytes, neurons, and capillaries with the pia, meninges and CSF. Vimentin expression is characteristic of glial cells that are rapidly dividing, such as radial glial cells during brain development (Noctor et al., 2002; Noctor, Flint, Weissman, Dammerman, & Kriegstein, 2001; Noctor, Martínez-Cerdeño, Ivic, & Kriegstein, 2004) and of glial cells undergoing morphological changes (Hutchins & Casagrande, 1989). We did not detect proliferative activity in ILA, so perhaps vimentin expression is linked to morphological modifications in ILA that we could not detect in static images. That is the case of $Vimentin^+$ Müller Glia of the adult retina that show changing morphology linked to their maturation state (Tsukahara, Umazume, McDonald, Kaplan, & Tamiya, 2017). in vitro

culture experiments could shed light into potential ILA morphological modifications in vivo. In addition to ILA, other cell types that express vimentin in the adult cortex are tanycytes. Tanycytes are ependymal cells whose soma form the wall of the lateral ventricle and allow communication between the ventricles and capillaries in the cortex. Accordingly, ILA may facilitate the communication of the cortex with capillaries, meninges and CSF. An alteration of any of these functions could contribute to disease. However, while protoplasmic astrocytes have been involved in neurodevelopmental diseases–Rett syndrome, Fragile X, Alexander disease, Epilepsy, and Autism-spectrum disorder (Molofsky et al., 2012; Schitine et al., 2015)–nothing is currently known about ILA involvement in disease, being this a matter that merits to be investigated in future studies.

5 | CONCLUSION

In conclusion, both pial and subpial ILA subtypes express GFAP and possess interlaminar processes, but these cells differ in soma morphology, spatial location, and presence in the cerebral cortex across species. Pial ILA are present in their rudimentary or typical form in all therian mammalian species, rudimentary subpial ILA are present in the ventral cortex of most eutherian mammals, while typical subpial ILA are only present in certain species of primate. Among primates, most interlaminar processes emerge from pial ILA, with a minority of processes arising from subpial ILA. The density of pial ILA is slightly increased in primates compared to other species, and the complexity of ILA is greatly increased in primates compared to other species. Pial ILA processes contact the pia, pial components, neuronal elements, and capillaries, suggesting a complex diverse functional repertoire for ILA.

ACKNOWLEDGMENTS

We thank Mackenzie Englund and Dr. Leah Krubitzer, Christopher Pivetti and Dr. Aijun Wang, Jeff Bennet and Dr. David Amaral, and Dr. Mary Ann Raghanti and the Cleveland Metroparks Zoo for donating tissue for this project. We thank Dr. Olga Chechneva for useful discussion.

Funding information

Shriners Hospitals

REFERENCES

Akiyama H, Tooyama I, Kawamata T, Ikeda K, & McGeer PL (1993). Morphological diversities of CD44 positive astrocytes in the cerebral cortex of normal subjects and patients with Alzheimer's disease. Brain Research, 632, 249–259. [PubMed: 7511977]

Andriezen WL (1893). The neuroglia elements in the human brain. British Medical Journal, 2, 227–230.

Ariza J, Rogers H, Hartvigsen A, Snell M, Dill M, Judd D, … Martínez-Cerdeño V (2017). Iron accumulation and dysregulation in the putamen in fragile X-associated tremor/ataxia syndrome. Movement Disorders: Official Journal of the Movement Disorder Society, 32, 585–591. [PubMed: 28233916]

Aspelund A, Antila S, Proulx ST, Karlsen TV, Karaman S, Detmar M, … Alitalo K (2015). A dural lymphatic vascular system that drains brain interstitial fluid and macromolecules. The Journal of Experimental Medicine, 212, 991–999. [PubMed: 26077718]

Bacyinski A, Xu M, Wang W, & Hu J (2017). The Paravascular pathway for brain waste clearance: Current understanding, significance and controversy. Frontiers in Neuroanatomy, 11.

Boya J, & Calvo JL (1993). Immunohistochemical study of the pineal astrocytes in the postnatal development of the cat and dog pineal gland. Journal of Pineal Research, 15, 13–20. [PubMed: 8229641]

Castellano B, González B, Jensen MB, Pedersen EB, Finsen BR, & Zimmer J (1991). A double staining technique for simultaneous demonstration of astrocytes and microglia in brain sections and astroglial cell cultures. The Journal of Histochemistry and Cytochemistry: Official Journal of the Histochemistry Society, 39, 561–568. [PubMed: 1707903]

Charvet CJ, Hof PR, Raghanti MA, Van Der Kouwe AJ, Sherwood CC, & Takahashi E (2017). Combining diffusion magnetic resonance tractography with stereology highlights increased cross-cortical integration in primates. The Journal of Comparative Neurology, 525, 1075–1093. [PubMed: 27615357]

Chen Y, Weng J, Han D, Chen B, Ma M, Yu Y, … Jiang B (2016). GSK3β inhibition accelerates axon debris clearance and new axon remyelination. American Journal of Translational Research, 8, 5410–5420. [PubMed: 28078012]

Colombo JA (1996). Interlaminar astroglial processes in the cerebral cortex of adult monkeys but not of adult rats. Acta Anatomica (Basel), 155, 57–62.

Colombo JA, Fuchs E, Hartig W, Marotte LR, & Puissant V (2000). “Rodent-like” and “primate-like” types of astroglial architecture in the adult cerebral cortex of mammals: A comparative study. Anatomy and Embryology, 201, 111–120. [PubMed: 10672363]

Colombo JA, Gayol S, Yañez A, & Marco P (1997). Immunocytochemical and electron microscope observations on astroglial interlaminar processes in the primate neocortex. Journal of Neuroscience Research, 48, 352–357. [PubMed: 9169861]

Colombo JA, Hartig W, Lipina S, & Bons N (1998). Astroglial interlaminar processes in the cerebral cortex of prosimians and Old World monkeys. Anatomy and Embryology, 197, 369–376. [PubMed: 9623670]

Colombo JA, Lipina S, Yáñez A, & Puissant V (1997). Postnatal development of interlaminar astroglial processes in the cerebral cortex of primates. International Journal of Developmental Neuroscience: The Official Journal of the International Society for Developmental Neuroscience, 15, 823–833. [PubMed: 9580494]

Colombo JA, & Puissant V (1994) Transitional glia and nonhomogeneities in cortical GFAP+ astroglia in adult Cebus apella monkeys. Proc 1st European Meeting on Glial cell function in health and disease, Heidelberg, p 74”

Colombo JA, & Reisin HD (2004). Interlaminar astroglia of the cerebral cortex: A marker of the primate brain. Brain Research, 1006, 126–131. [PubMed: 15047031]

Colombo JA, Reisin HD, Miguel-Hidalgo JJ, & Rajkowska G (2006). Cerebral cortex astroglia and the brain of a genius: A propos of a. Einstein’s. Brain Research Reviews, 52, 257–263. [PubMed: 16675021]

Colombo JA, Schleicher A, & Zilles K (1999). Patterned distribution of immunoreactive astroglial processes in the striate (V1) cortex of New World monkeys. Glia, 25, 85–92. [PubMed: 9888300]

Colombo JA, Sherwood CC, & Hof PR (2004). Interlaminar astroglial processes in the cerebral cortex of great apes. Anatomy and Embryology, 208, 215–218. [PubMed: 15221474]

Colombo JA, Yáñez A, Puissant V, & Lipina S (1995). Long, interlaminar astroglial cell processes in the cortex of adult monkeys. Journal of Neuroscience Research, 40, 551–556. [PubMed: 7616615]

Dai X, Jiang W, Zhang Q, Xu L, Geng P, Zhuang S, … Liang X (2013). Requirement for integrin-linked kinase in neural crest migration and differentiation and outflow tract morphogenesis. BMC Biology, 11, 107. [PubMed: 24131868]

Dell L-A, Karlsson KA, Patzke N, Spocter MA, Siegel JM, & Manger PR (2016a). Organization of the sleep-related neural systems in the brain of the minke whale (Balaenoptera acutorostrata). The Journal of Comparative Neurology, 524, 2018–2035. [PubMed: 26588800]

Dell L-A, Patzke N, Spocter MA, Siegel JM, & Manger PR (2016b). Organization of the sleep-related neural systems in the brain of the harbour porpoise (Phocoena phocoena). The Journal of Comparative Neurology, 524, 1999–2017. [PubMed: 26588354]

Du J, Zhang C, Na X, Li A, Zhang Q, Li K, & Ding Y (2018). Andro-grapholide protects mouse astrocytes against hypoxia injury by promoting autophagy and S100B expression. Brazilian Journal of Medical and Biological Research, 51, e7061. [PubMed: 29694508]

Garcia-Esparcia P, Diaz-Lucena D, Ainciburu M, Torrejón-Escribano B, Carmona M, Llorens F, & Ferrer I (2018). Glutamate transporter GLT1 expression in Alzheimer disease and dementia with Lewy bodies. Frontiers in Aging Neuroscience, 10.

Hansen SH, Stagaard M, & Møllgård K (1989). Neurofilament-like pattern of reactivity in human foetal PNS and spinal cord following immunostaining with polyclonal anti-glial fibrillary acidic protein antibodies. Journal of Neurocytology, 18, 427–436. [PubMed: 2681541]

Hashemi E, Ariza J, Rogers H, Noctor SC, & Martínez-Cerdeño V (2017). The number of Parvalbumin-expressing interneurons is decreased in the medial prefrontal cortex in autism. Cerebral Cortex, 1991(27), 1931–1943.

Hubbard JA, Hsu MS, Seldin MM, & Binder DK (2015). Expression of the astrocyte water channel aquaporin-4 in the mouse brain. ASN Neuro, 7, 175909141560548.

Hutchins JB, & Casagrande VA (1989). Vimentin: Changes in distribution during brain development. Glia, 2, 55–66. [PubMed: 2523339]

Iliff JJ, Wang M, Liao Y, Plogg BA, Peng W, Gundersen GA, … Nedergaard M (2012). A Paravascular pathway facilitates CSF flow through the brain parenchyma and the clearance of interstitial solutes, including amyloid p. Science Translational Medicine, 4, 147ra–111.

Kanazawa H, Ohsawa K, Sasaki Y, Kohsaka S, & Imai Y (2002). Macrophage/microglia-specific protein Iba1 enhances membrane ruffling and Rac activation via phospholipase C-gamma - dependent pathway. The Journal of Biological Chemistry, 277, 20026–20032. [PubMed: 11916959]

Korzhevskii DE, Otellin VA, & Grigor'ev IP (2005). Glial fibrillary acidic protein in astrocytes in the human neocortex. Neuroscience and Behavioral Physiology, 35, 789–792. [PubMed: 16132257]

Krzisch M, Temprana SG, Mongiat LA, Armida J, Schmutz V, Virtanen MA, … Toni N (2015). Pre-existing astrocytes form functional perisynaptic processes on neurons generated in the adult hippocampus. Brain Structure & Function, 220, 2027–2042. [PubMed: 24748560]

Li W, Li K, Gao J, & Yang Z (2018). Autophagy is required for human umbilical cord mesenchymal stem cells to improve spatial working memory in APP/PS1 transgenic mouse model. Stem Cell Research & Therapy, 9, 9. [PubMed: 29335016]

Lin N-H, Messing A, & Perng M-D (2017). Characterization of a panel of monoclonal antibodies recognizing specific epitopes on GFAP. PLoS One, 12, e0180694. [PubMed: 28700643]

Loganathan K, Salem Said E., Winterrowd E, Orebrand M, He L, Vanlandewijck M, … Jeansson M (2018). Angiopoietin-1 deficiency increases renal capillary rarefaction and tubulointerstitial fibrosis in mice. PLoS One, 13, e0189433. [PubMed: 29293543]

Louveau A, Smirnov I, Keyes TJ, Eccles JD, Rouhani SJ, Peske JD, … Kipnis J (2015). Structural and functional features of central nervous system lymphatics. Nature, 523, 337–341. [PubMed: 26030524]

Lundgaard I, Luzhynskaya A, Stockley JH, Wang Z, Evans KA, Swire M, et al. (2013). Neuregulin and BDNF induce a switch to NMDA receptor-dependent myelination by oligodendrocytes. PLoS Biology, 11, e1001743. [PubMed: 24391468]

Makino S, Zhulyn O, Mo R, Puviindran V, Zhang X, Murata T, … Gondo Y (2015). T396I mutation of mouse Sufu reduces the stability and activity of Gli3 repressor. PLoS One, 10, e0119455. [PubMed: 25760946]

Manger PR, Pillay P, Maseko BC, Bhagwandin A, Gravett N, Moon D-J, … Hemingway J (2009). Acquisition of brains from the African elephant (Loxodonta africana): Perfusion-fixation and dissection. Journal of Neuroscience Methods, 179, 16–21. [PubMed: 19168095]

Martínez-Cerdeño V, Camacho J, Ariza J, Rogers H, Horton-Sparks K, Kreutz A, … Noctor SC (2017). The bat as a new model of cortical development. Cerebral Cortex, 28(11), 3880–3893.

Martínez-Cerdeño V, Cunningham CL, Camacho J, Keiter JA, Ariza J, Lovern M, & Noctor SC (2016). Evolutionary origin of Tbr2-expressing precursor cells and the subventricular zone in the developing cortex. The Journal of Comparative Neurology, 524, 433–447. [PubMed: 26267763]

McTigue DM, Wei P, & Stokes BT (2001). Proliferation of NG2-positive cells and altered oligodendrocyte numbers in the contused rat spinal cord. Journal of Neuroscience: The Official Journal of the Society for Neuroscience, 21, 3392–3400.

Molofsky AV, Krencik R, Krenick R, Ullian EM, Ullian E, Tsai H, … Rowitch DH (2012). Astrocytes and disease: A neurodevelopmental perspective. Genes & Development, 26, 891–907. [PubMed: 22549954]

Mukhopadhyay A, Jarrett J, Chlon T, & Kessler JA (2009). HeyL regulates the number of TrkC neurons in dorsal root ganglia. Developmental Biology, 334, 142–151. [PubMed: 19631204]

Noctor SC, Flint AC, Weissman TA, Dammerman RS, & Kriegstein AR (2001). Neurons derived from radial glial cells establish radial units in neocortex. Nature, 409, 714–720. [PubMed: 11217860]

Noctor SC, Flint AC, Weissman TA, Wong WS, Clinton BK, & Kriegstein AR (2002). Dividing precursor cells of the embryonic cortical ventricular zone have morphological and molecular characteristics of radial glia. Journal of Neuroscience: The Official Journal of the Society for Neuroscience, 22, 3161–3173.

Noctor SC, Martínez-Cerdeño V, Ivic L, & Kriegstein AR (2004). Cortical neurons arise in symmetric and asymmetric division zones and migrate through specific phases. Nature Neuroscience, 7,136–144. [PubMed: 14703572]

Oberheim NA, Takano T, Han X, He W, Lin JHC, Wang F, … Nedergaard M (2009). Uniquely hominid features of adult human astrocytes. Journal of Neuroscience: The Official Journal of the Society for Neuroscience, 29, 3276–3287.

Oberheim NA, Wang X, Goldman S, & Nedergaard M (2006). Astrocytic complexity distinguishes the human brain. Trends in Neurosciences, 29, 547–553. [PubMed: 16938356]

Pelletier J, Agonsanou H, Delvalle N, Fausther M, Salem M, Gulbransen B, & Sévigny J (2017). Generation and characterization of polyclonal and monoclonal antibodies to human NTPDase2 including a blocking antibody. Purinergic Signal, 13, 293–304. [PubMed: 28409324]

Pillai AG, de Jong D, Kanatsou S, Krugers H, Knapman A, Heinzmann J-M, … Touma C (2012). Dendritic morphology of hippocampal and amygdalar neurons in adolescent mice is resilient to genetic differences in stress reactivity. PLoS One, 7, e38971. [PubMed: 22701737]

Ramón y Cajal S (1904). Glial cells of the cerebral cortex of a child. In Ink and pencil on paper. Madrid: Instituto Cajal.

Retzius G (1894). Biologische Untersuchungen Die Neuroglia des Gehirns beim Menschen und bei Saeugethieren, Vol. 6, Verlag von Gustav Fischer, Jena.

Rutka JT, Murakami M, Dirks PB, Hubbard SL, Becker LE, Fukuyama K, … Matsuzawa K. (1997). Role of glial filaments in cells and tumors of glial origin: A review. Journal of Neurosurgery, 87, 420–430. [PubMed: 9285609]

Sasai N, Kutejova E, & Briscoe J (2014). Integration of signals along orthogonal axes of the vertebrate neural tube controls progenitor competence and increases cell diversity. PLoS Biology, 12, e1001907. [PubMed: 25026549]

Schitine C, Nogaroli L, Costa MR, & Hedin-Pereira C (2015). Astrocyte heterogeneity in the brain: From development to disease. Frontiers in Cellular Neuroscience, 9, 76. [PubMed: 25852472]

Scuderi C, Stecca C, Iacomino A, & Steardo L (2013). Role of astrocytes in major neurological disorders: The evidence and implications. IUBMB Life, 65, 957–961. [PubMed: 24376207]

Sofroniew MV, & Vinters HV (2010). Astrocytes: Biology and pathology. Acta Neuropathology, 119, 7–35.

Sosunov AA, Wu X, Tsankova NM, Guilfoyle E, McKhann GM, & Goldman JE (2014). Phenotypic heterogeneity and plasticity of isocortical and hippocampal astrocytes in the human brain. Journal of Neuroscience: The Official Journal of the Society for Neuroscience, 34, 2285–2298.

Tsukahara R, Umazume K, McDonald K, Kaplan HJ, & Tamiya S (2017). Focal adhesion kinase family is involved in matrix contraction by transdifferentiated Müller cells. Experimental Eye Research, 164, 90–94. [PubMed: 28818394]

Vasile F, Dossi E, & Rouach N (2017). Human astrocytes: Structure and functions in the healthy brain. Brain Structure & Function, 222, 2017–2029. [PubMed: 28280934]

Werner A, Iwasaki S, McGourty C, Medina-Ruiz S, Teerikorpi N, Fedrigo I, … Rape M (2015). Cell fate determination by ubiquitin-dependent regulation of translation. Nature, 525, 523–527. [PubMed: 26399832]

Zeng HK, Wang QS, Deng YY, Fang M, Chen CB, Fu YH, … Jiang X (2010). Hypertonic saline ameliorates cerebral edema through downregulation of aquaporin-4 expression in the astrocytes. Neuroscience, 166, 878–885. [PubMed: 20083168]

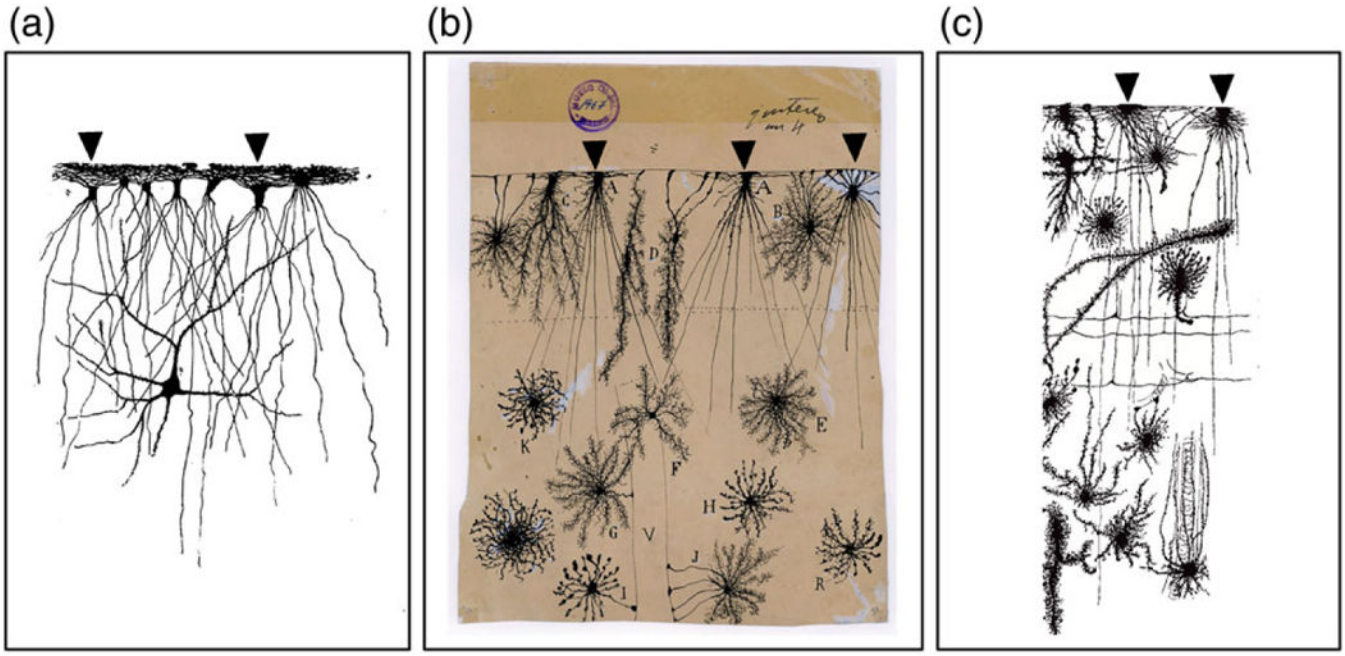

FIGURE 1.

Summary of previous studies on ILA (a–c) Previous description of ILA (a) Representation of “caudate cells” observed by Andriezen, adapted from “The neuroglia elements in the human brain,” by W. L. Andriezen, 1893, British Medical Journal, 2, pp. 227–230, (b) Representation of morphological diversity of glial cells in human cerebral cortex- including ILA-, adapted from (Ramón y Cajal, 1904), and (c) (Retzius, 1894) [Color figure can be viewed at wileyonlinelibrary.com]

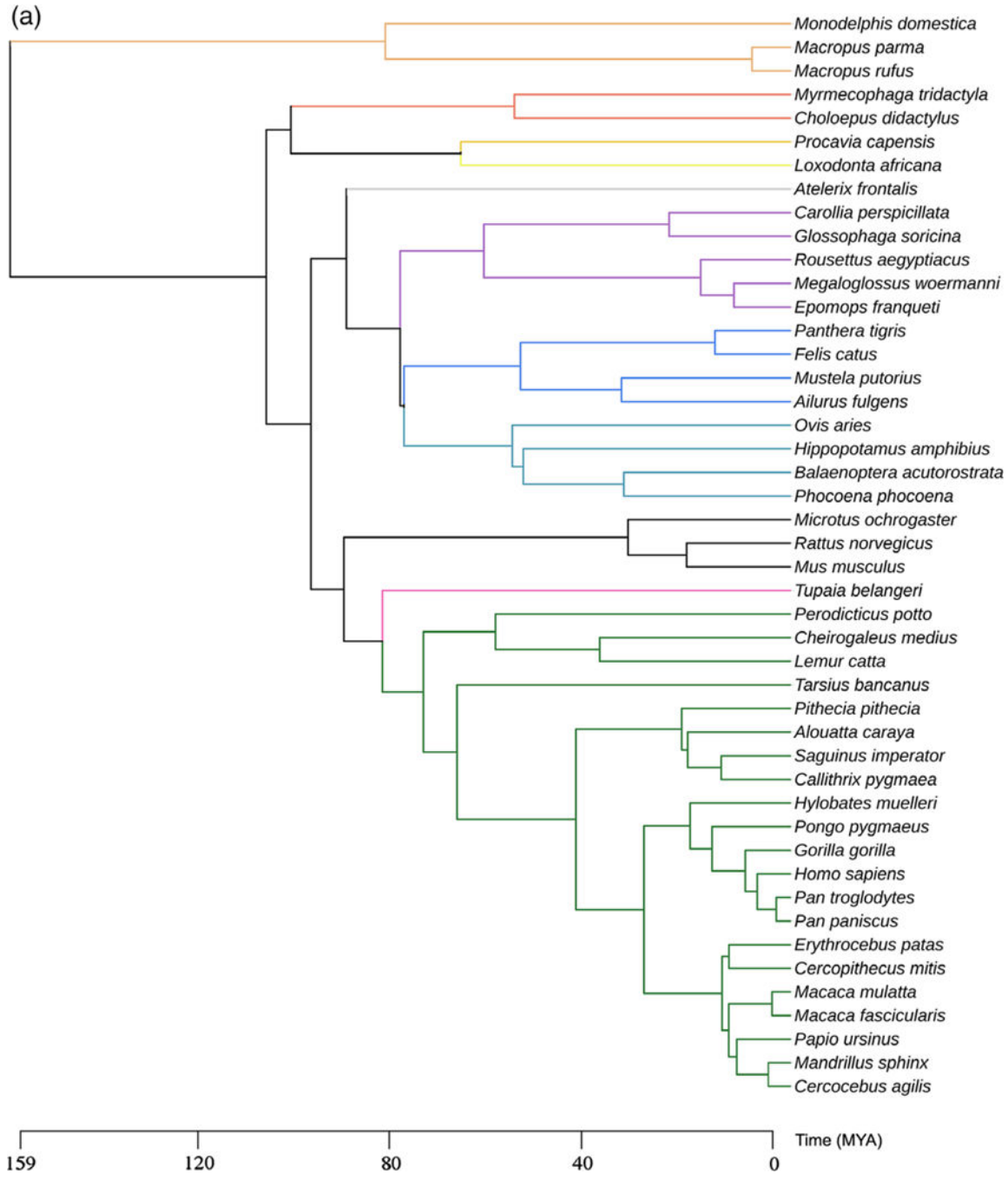

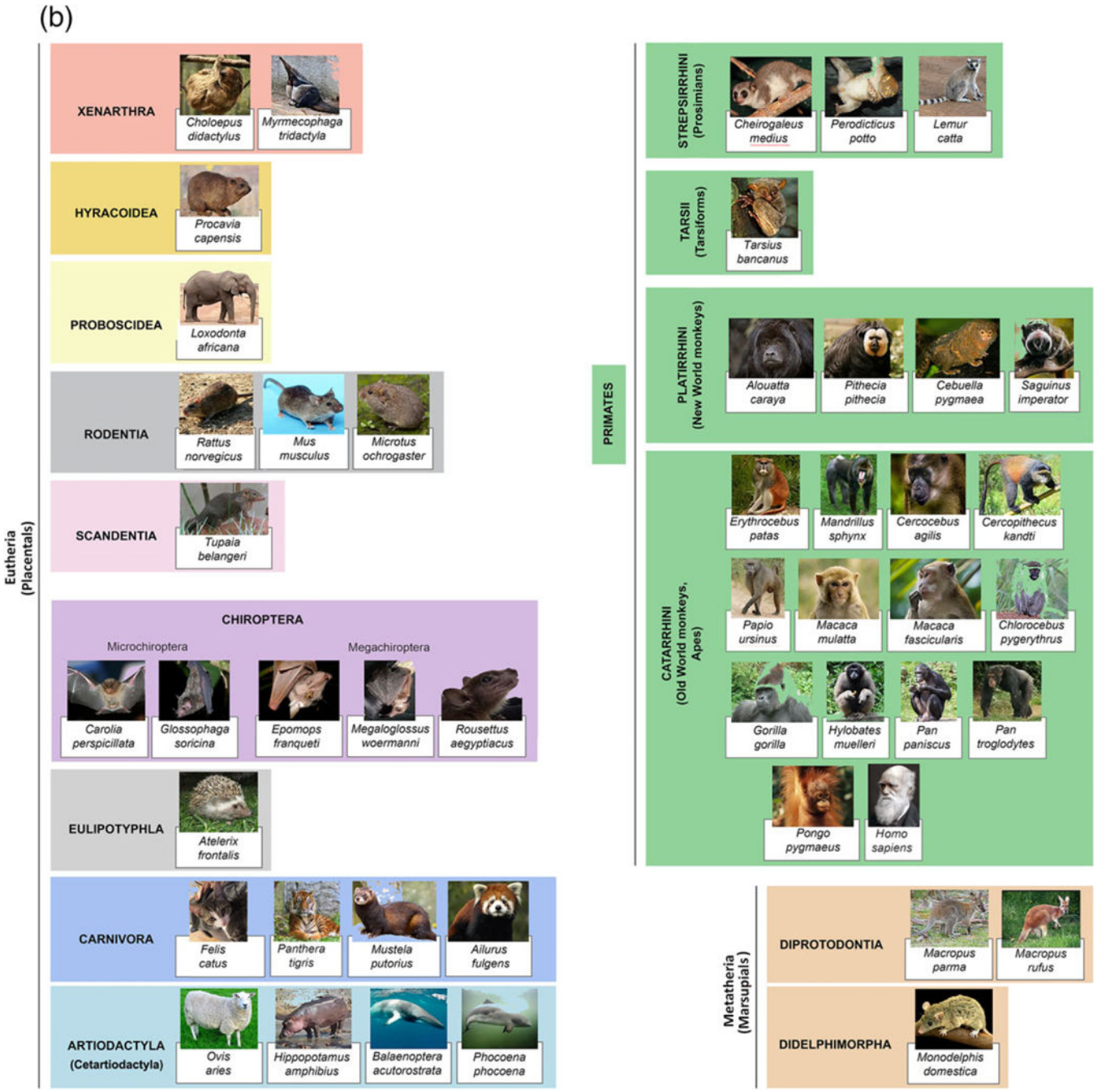

FIGURE 2.

Taxonomy of the species included in this study. (a) Evolutionary map and (b) Graphic illustration of single species [Color figure can be viewed at wileyonlinelibrary.com]

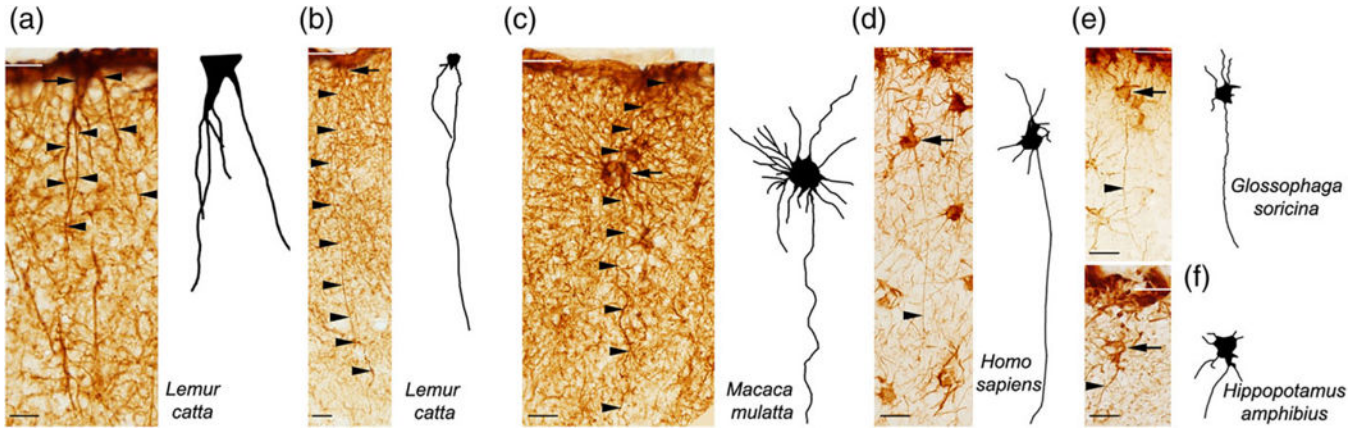

FIGURE 3.

Pial and subpial ILA. Pial ILA have an inverted pyramidal shape with the base of the soma contacting the pia. In contrast, subpial ILA are multipolar cells with a round or oval soma that is located in the lower part of the upper layer I and does not touch the pia. (a-f) $GFAP^{+}$ pial and subpial ILA, with their respective 2D reconstruction. Black arrows and arrowheads point at ILA somas and processes, respectively. White lines indicate pial surface. Scale bars = (a) 25 μm, (b) 50 μm, (c–f) 25 μm [Color figure can be viewed at wileyonlinelibrary.com]

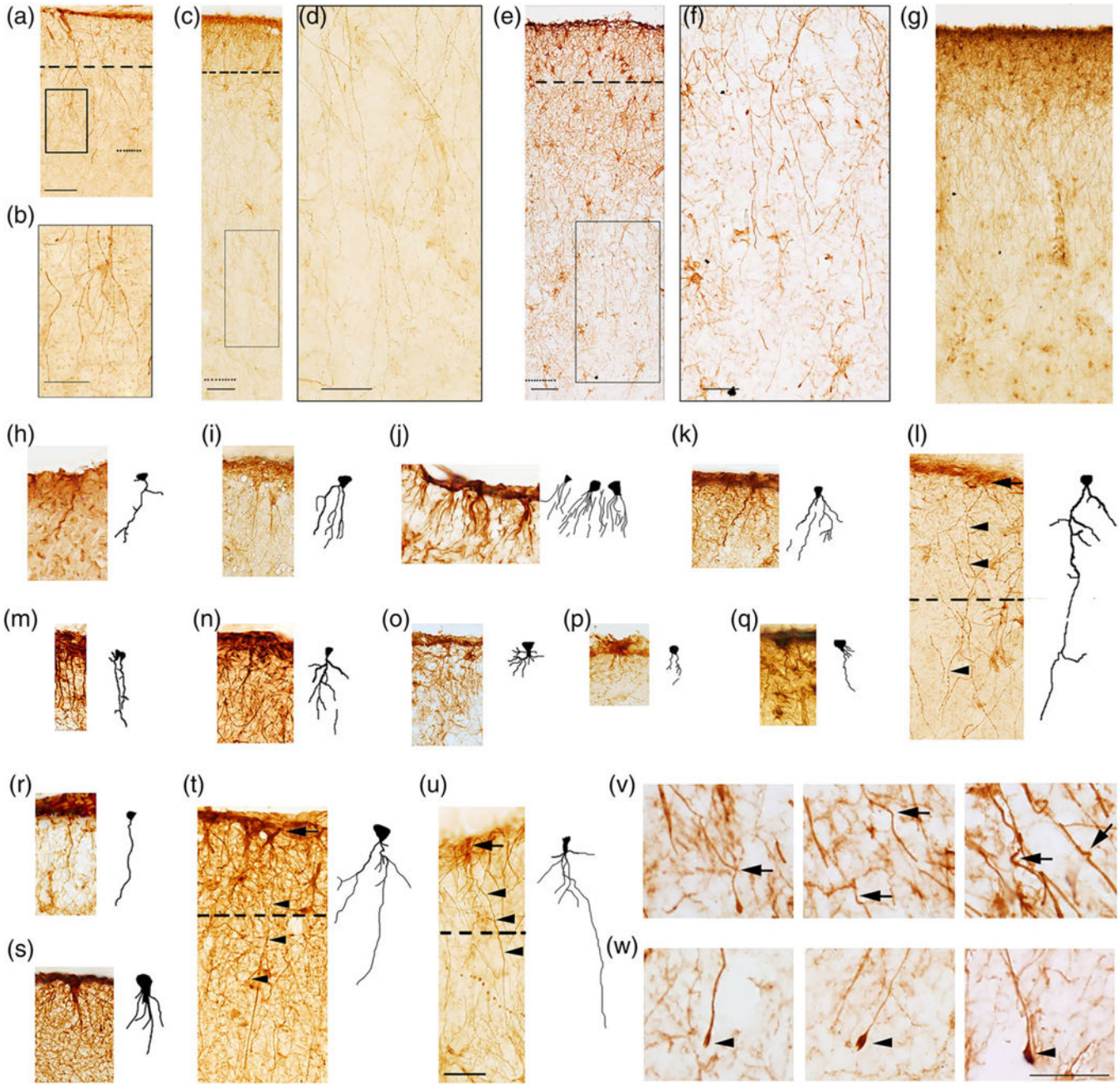

FIGURE 4.

Pial ILA morphology in mammals. GFAP^{+} pial ILA in (a) *Procavia capensis* dorsal cortex (c) *Pan paniscus* dorsal cortex, (e) *Homo sapiens* dorsal cortex. Dashed line indicates layer I boundary. (b, d, f) higher magnification of black squares in (a, c, and e), respectively. (g) *Pan paniscus* dorsal cortex, example of palisade. Dotted line indicates: (a) layer II-III boundary (c, e) layer III-IV boundary. (h–u) ILA+ rudimentary and mature pial ILA in: (h) *Monodelphis domestica,* (i) *Choloepus didactylus,* (j) *Mus musculus,* (k) *Rattus norvegicus,* (l) *Procavia capensis,* (m) *Carollia perspicillata,* (n) *Glossophaga soricina,* (o) *Epomops franqueti,* (p) *Megaloglossus woermanni,* (q) *Felis catus,* (r) *Ailurus fulgens,* (s) *Lemur*

catta, (t) *Macaca mulatta,* (u) *Pan paniscus,* with their respective 2D reconstruction. Dashed line indicates layer I boundary. Black arrows and black arrowheads point at ILA somata and processes, respectively. (v, w) Curves (black arrows) and terminal bulbs (black arrowheads) of human ILA processes, respectively. Scale bars = (a, c, e, h–u) 50 μm, (b, d, f) 25 μm, and (v, w) 20 μm [Color figure can be viewed at wileyonlinelibrary.com]

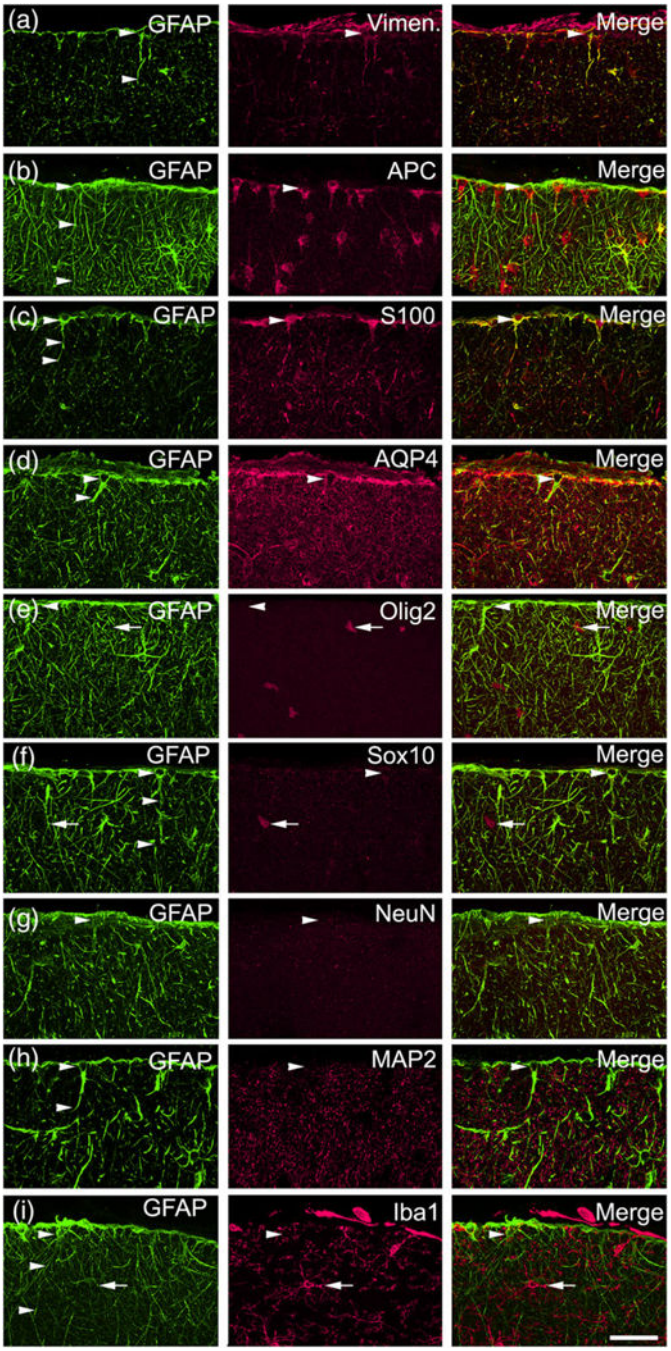

FIGURE 5.

ILA molecular characterization in rhesus macaque (*Macaca mulatta*) cerebral cortex. ILA express Vimentin, APC, S100β, AQP4, and do not express Olig2, Sox10, NeuN, MAP2, Iba1. (a) GFAP (green)–Vimentin (red), (b) GFAP (green)–APC (red), (c) GFAP (green)–S100β (red), (d) GFAP (green)–AQP4 (red), (e) GFAP (green)–Olig2 (red), (f) GFAP (green)–Sox10 (red), (g) GFAP (green)–NeuN (red), (h) GFAP (green)–MAP2 (red), (i) GFAP (green)–Iba1 (red). White arrowheads point at ILA cells (somata and/or processes), positive for: Vimentin, APC, S100β, AQP4, and negative for: Olig2, Sox10, NeuN, MAP2,

Iba1. White arrows pointing at Olig2^{+} cells (e), Sox10^{+} cells (f), Iba1^{+} cells (h). Scale bar = 50 μm [Color figure can be viewed at wileyonlinelibrary.com]

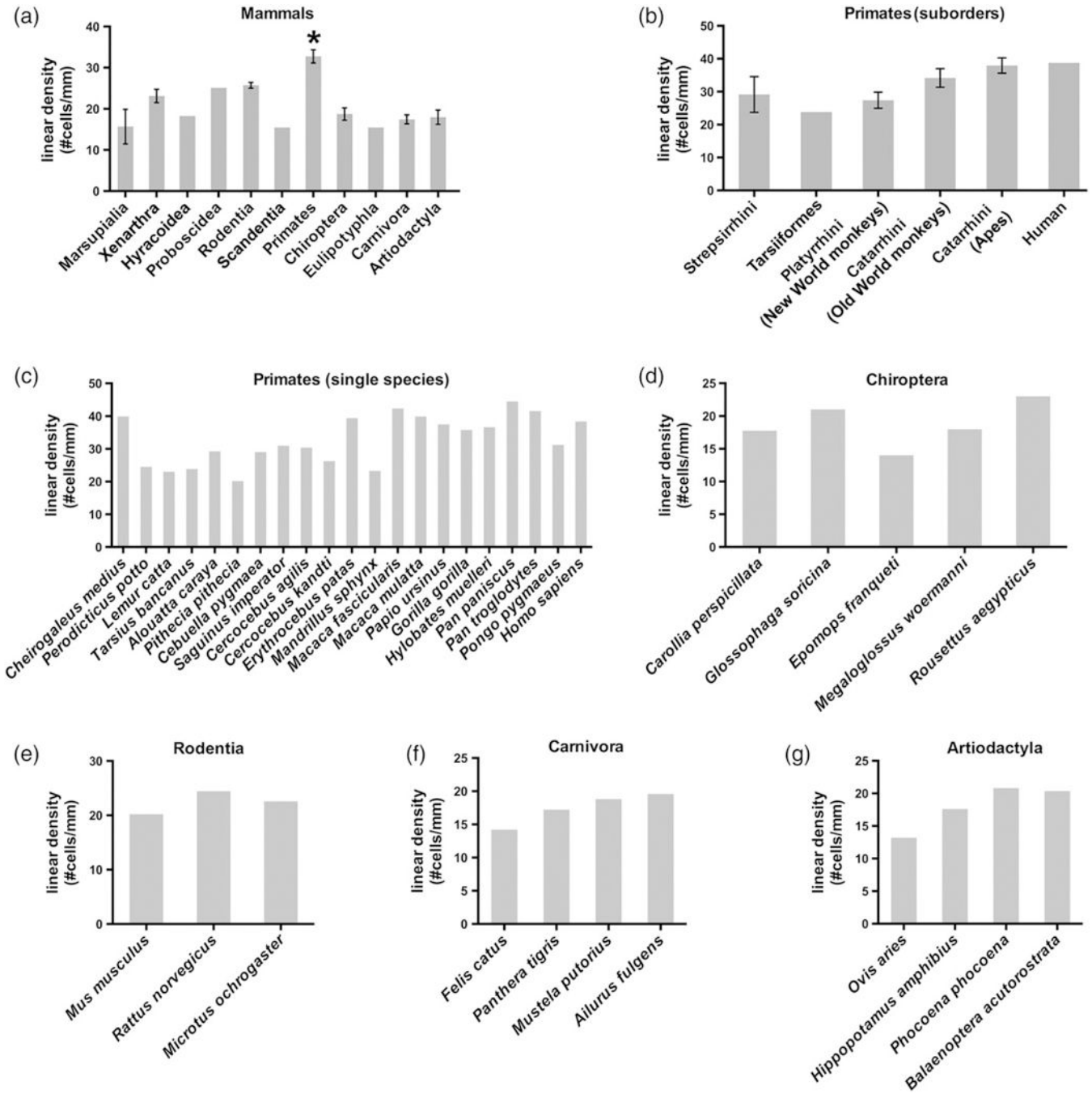

FIGURE 6.

ILA linear density across evolution. ILA linear density (evaluated as number of pial ILA cells divided per mm) in: (a) Mammalian orders. *t*-test as follows: primates versus marsupials: $p < .002$; primates versus rodentia: $p < .01$; primates versus chiropterans: $p < .0002$; primate versus Carnivora: $p < .0003$; primates versus artiodactyls: $p < .0002$. (b) Primate suborders (c) Primate species. (d–g) ILA linear density in chiropterans, rodents, carnivores, and artiodactyls species

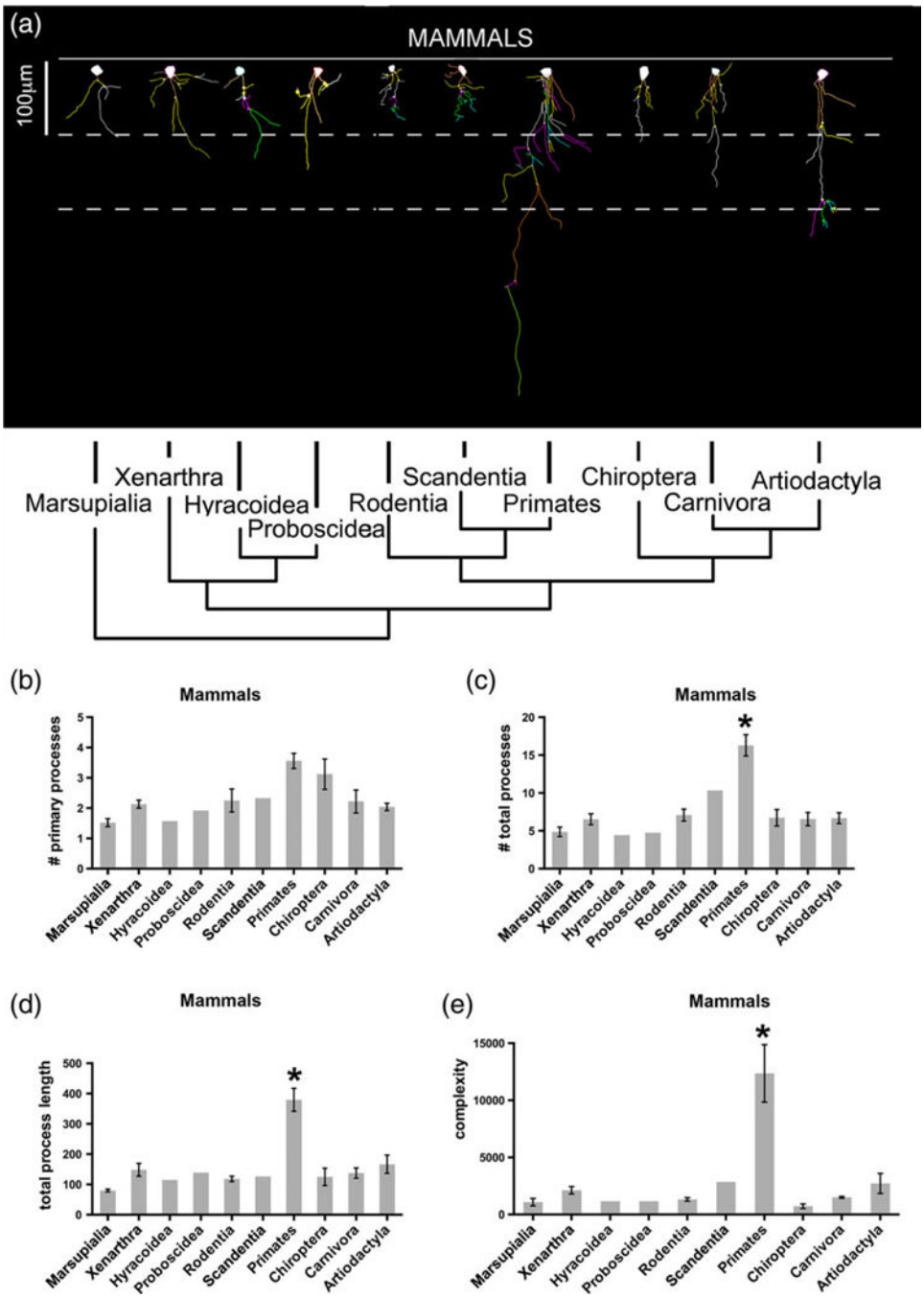

FIGURE 7.

ILA morphology in mammalian species. Representation of ILA morphology from the species with the longest interlaminar process (dorsal or ventral) belonging to each order. (a) Neurolucida 2D reconstruction. (b–e) Number of primary processes, total number of processes, total process length, and complexity index in ILA in mammalian orders. *t*-test as follows: Primates versus marsupials: (b) $p < .004$, (c) $p < .03$, (d) $p < .004$, (e) $p < .05$; primates versus xenarthra: (b) $p < .05$, (c) $p < .02$, (d) $p < .04$, (e) $p < .06$; primates versus rodents: (a) $p < .04$, (c) $p < .01$, (d) $p < .009$, (e) $p < .05$; primates versus chiropterans: (c) p

< .002, (d) p < .002, (e) p < .02; primates versus carnivores: (b) p < .02, (c) p < .004, (d) p < .006, (e) p < .04; primates versus artiodactyls: (b) p < .009, (c) p < .004, (d) p < .01, (e) p < .05. Scale bar = 100 μm [Color figure can be viewed at wileyonlinelibrary.com]

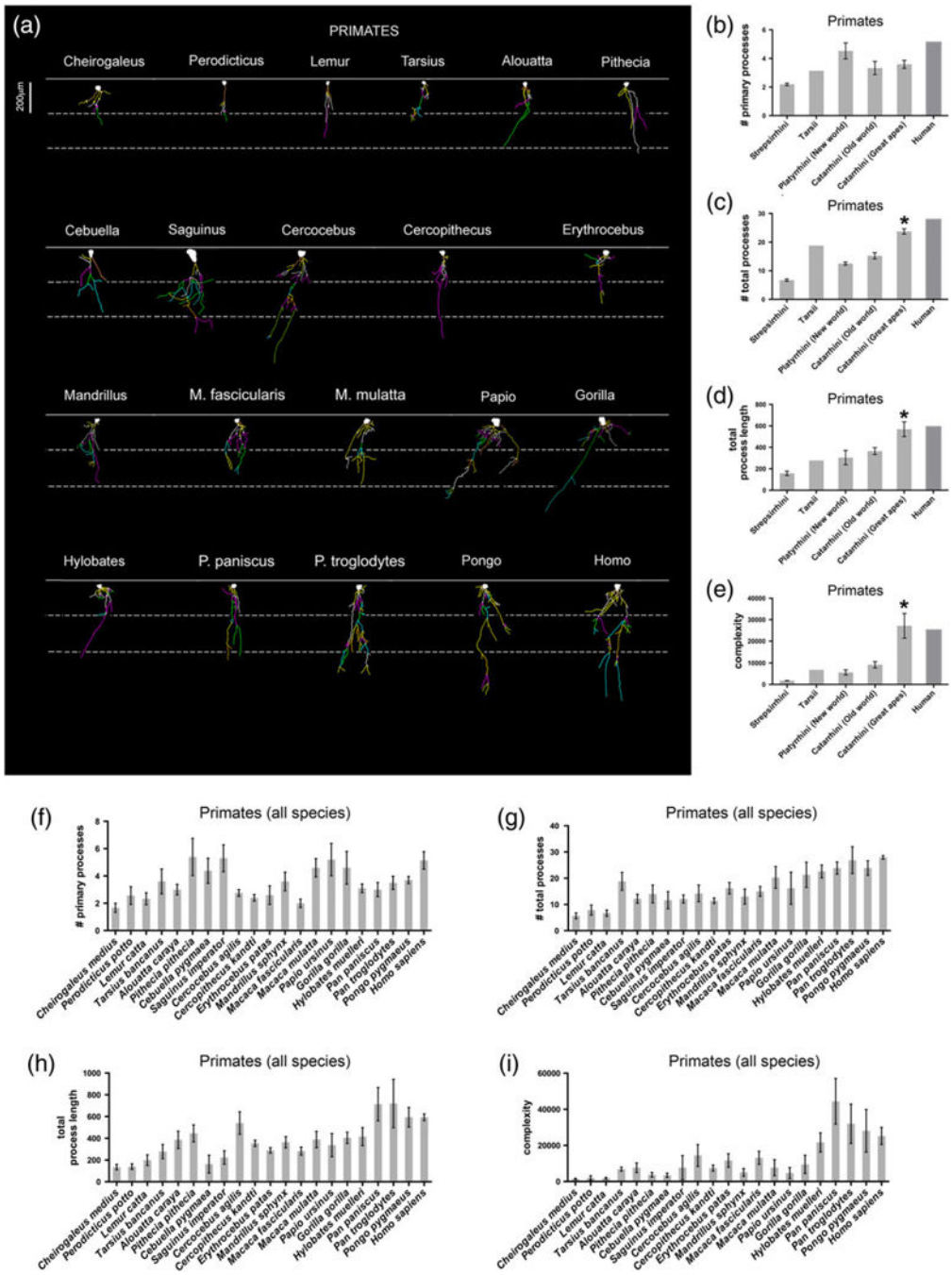

FIGURE 8.

ILA morphological diversity in primates. Representation of ILA morphology from the species with the longest dorsal interlaminar process belonging to each order. (a) Neurolucida 2D reconstruction samples. (b–i) Number of primary processes, total number of processes, total process length, and complexity index in ILA, in: (b–e) Primate suborders, and (f–i) Single primate species. Scale bar = 200 μm [Color figure can be viewed at wileyonlinelibrary.com]

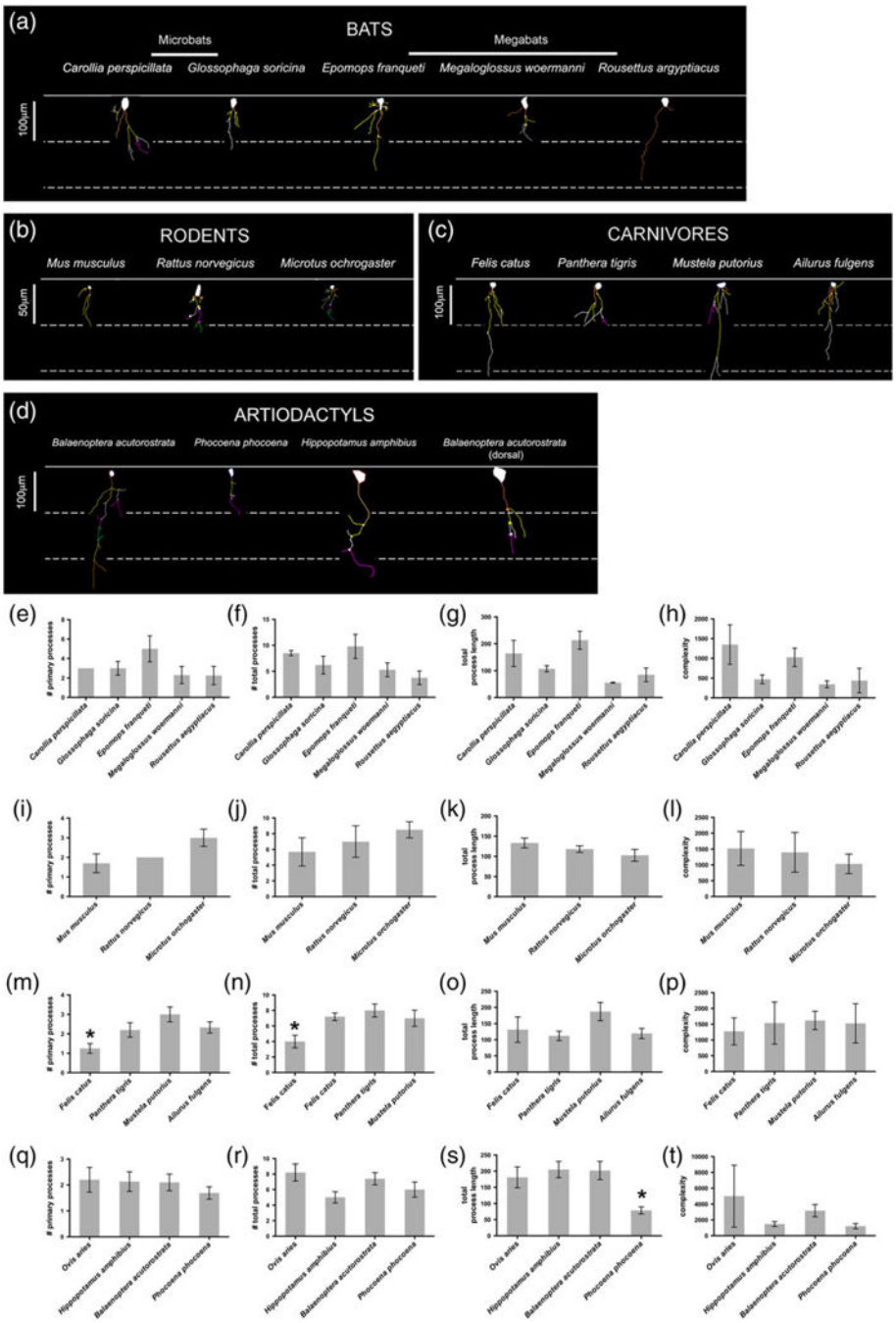

FIGURE 9.

ILA morphological diversity. Representation of ILA morphology from the species with the longest ventral interlaminar process belonging to each order. ILA Neurolucida 2D reconstruction samples of: (a) Chiropterans (ventral cortex), (b) Rodents, (c) Carnivores, (d) Artiodactyls. Number of primary processes, total number of processes, total process length, and complexity index in ILA in: (e–h) Chiropterans, (i–l) rodents, (m–p) carnivores, (q–t) artiodactyls. Scale bar in (a) 100 µm, in (b) 50 µm, (c) 100 µm, (d) 100 µm [Color figure can be viewed at wileyonlinelibrary.com]

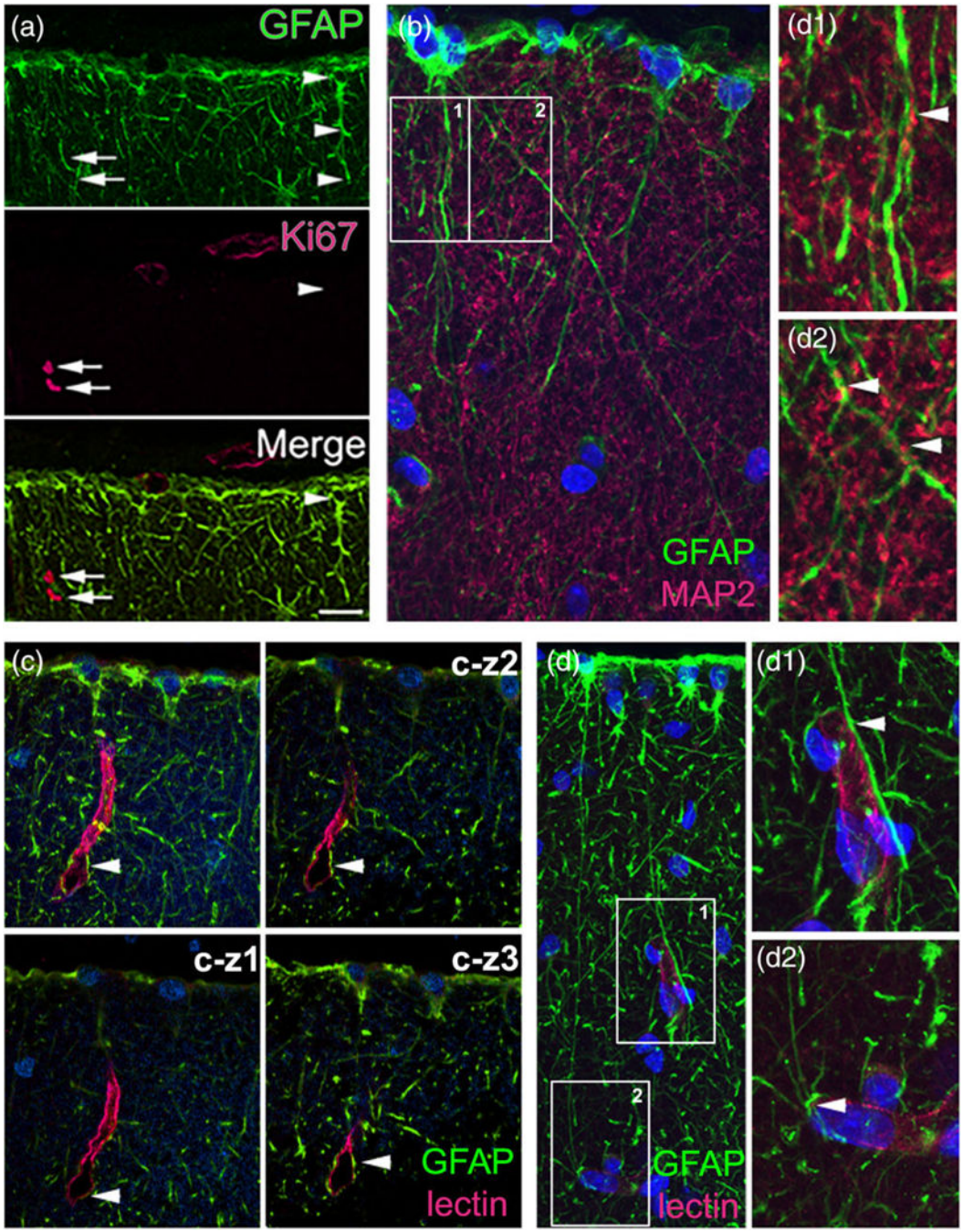

FIGURE 10.

ILA contact neuronal processes and capillaries. Double immunofluorescence staining in *Macaca mulatto* cerebral cortex. (a) ILA do not express the proliferative marker Ki67. GFAP (green)–Ki67 (red), 60x oil picture, (b) ILA contact neuropil. GFAP (green)–MAP2 (red), 100x oil picture. (b1–2) zoom of white squares in (b). (c, d) ILA contact lectin+ capillaries, 60x and 100x oil pictures, respectively. GFAP (green)–Lectin (red). (c-z1–3) individual images for the Z-stack for (c). (d1–2) zoom of white squares in (d). White arrowheads point to ILA cells in (a), and at $GFAP^+/MAP2^+$, and $GFAP^+/Lectin^+$ co-localization in (b) and

(c,d), respectively. White arrows point to $Ki67^{+}/GFAP^{-}$ cells in (a). Scale bars = (a) 50 μm, (b,d) 10 μm, (c) 20 μm [Color figure can be viewed at wileyonlinelibrary.com]

TABLE 1

Pial and subpial ILA presence in mammalian species analyzed. Highlighted in red are the species where proper subpial ILA are present

					Pial ILA		Subpial ILA	
Infraclass	**Order**	**Suborder Parvorder**	**Family**	**Species**	**D**	**V**	**D**	**V**
Metatheria (marsupials)								
	Diprotodontia		Macropodidae	*Macropus parma*	No	r	No	No
				Macropus rufus	No	r	No	No
	Didelphi-morphia		Didelphidae	*Monodelphis domestica*	No	r	No	No
Eutheria (Placentals)								
	Xenarthra		Megalonychidae	*Choloepus didactylus*	r	Yes	r	r
			Myrmecophagidae	*Myrmecophaga tridactyla*	r	-	No	-
	Hyracoidea		Procaviidae	*Procavia capensis*	Yes	Yes	r	r
	Proboscidea		Elephantidae	*Loxodonta africana*	Yes	Yes	No	r
	Rodentia	Myomorpha	Muridae	*Mus Musculus*	r	r	No	r
				Rattus norvegicus	r	r	No	r
		Muroidea	Cricetidae	*Microtus orchogaster*	r	r	No	No
	Scandentia		Tupaiidae	*Tupaia belangeri*	r	Yes	r	r
	Primates	Strepsirrhini	Cheirogaleidae	*Cheirogaleus medius*	Yes	Yes	r	r
			Lorisidae	*Perodicticus potto*	Yes	Yes	r	r
			Lemuridae	*Lemur catta*	Yes	Yes	r	r
		Tarsiiformes	Tarsiidae	*Tarsius bancanus*	Yes	Yes	r	r
		Haplorhini, Platyrrhini	Atelidae	*Alouatta Caraya*	Yes	Yes	Yes	Yes
			Pitheciidae	*Pithecia Pithecia*	Yes	Yes	r	Yes
			Callitrichidae	*Cebuella pygmaea*	Yes	Yes	r	r
				Saguinus imperator	Yes	Yes	r	r
		Haplorhini, Catarhhini	Cercopithecidae	*Cercocebus agilis*	Yes	-	Yes	-
				Cercopithecus kandti	Yes	Yes	r	Yes
				Erythrocebus patas	Yes	Yes	r	Yes
				Mandrillus sphynx	Yes	Yes	Yes	Yes
				Macaca fascicularis	Yes	Yes	r	Yes
				Macaca Mulatta	Yes	Yes	r	Yes

					Pial ILA		Subpial ILA	
Infraclass	**Order**	**Suborder Parvorder**	**Family**	**Species**	**D**	**V**	**D**	**V**
				Chlorocebus pygerythrus	Yes	Yes	r	Yes
				Papio Ursinus	Yes	Yes	Yes	Yes
			Hominidae	*Gorilla Gorilla*	Yes	Yes	Yes	Yes
				Hylobates muelleri	Yes	Yes	Yes	Yes
				Pan Paniscus	Yes	Yes	Yes	Yes
				Pan Troglodytes	Yes	Yes	Yes	Yes
				Pongo pygmaeus	Yes	Yes	Yes	Yes
				Homo Sapiens	Yes	-	Yes	-
	Chiroptera	Micro-chiroptera	Phyllostomidae	*Carollia perspicillata*	r	Yes	No	r
				Glossophaga soricina	r	Yes	No	r
		Mega-chiroptera	Pteropodidae	*Epomops franqueti*	r	Yes	No	r
				Megaloglossus woermanni	r	Yes	No	No
				Rousettus aegyptiacus	r	Yes	No	r
	Eulipotyphla		Erinaceidae	*Atelerix Frontalis*	No	p	No	No
	Carnivora	Feliformia	Felidae	*Felis Catus*	r	Yes	r	r
				Panthera Tigris	r	Yes	No	r
		Musteloidea	Mustelidae	*Mustela putorius*	r	Yes	r	r
		Caniformia	Ailuridae	*Ailurus Fulgens*	r	Yes	No	r
	Artiodactyla	Ruminantia	Bovidae	*Ovis Aries*	r	-	No	-
		Whippo-morpha	Hippopotamidae	*Hippopotamus amphibius*	No	r	No	r
		Cetacea	Balaenopteridae	*Balaenoptera acutorostrata*	r	Yes	No	No
			Phocoenidae	*Phocoena phocoena*	r	Yes	No	r

D = dorsal; V = ventral; r = rudimentary.

TABLE 2

ILA linear density, number of primary processes, number of total processes, total length, and complexity, of mammalian species analyzed

Infra-class	Order	Suborder, Parvorder	Family	Species	A	B	C	D	E
Metatheria (marsupials)									
	Diprotodontia		Macropodidae	*Macropus parma*	11.4	1.8	4.3	79.1	660.9
				Macropus rufus		1.5	4.3	87.5	878.9
	Didelphimorphia		Didelphidae	*Monodelphis domestica*	20.0	1.3	6.1	71.5	1,710.5
Eutheria (Placentals)									
	Xenarthra		Megalonychidae	*Choloepus didactylus*	21.5	2.0	5.8	169.4	1,798.5
			Myrmeco-phagidae	*Myrmecophaga tridactyla*	24.8	2.3	7.3	127.1	2,447.1
	Hyracoidea		Procaviidae	*Procavia capensis*	18.3	1.6	4.4	114.3	1,124.5
	Proboscidea		Elephantidae	*Loxodonta africana*	25.1	1.9	4.8	139.0	1,162.0
	Rodentia	Myomorpha	Muridae	*Mus musculus*	20.2	1.8	5.8	133.4	1,521.1
				Rattus norvegicus	24.4	2.0	7.0	118.5	1,398.2
		Muroidea	Cricetidae	*Microtus orchogaster*	22.6	3.0	8.5	102.8	1,034.1
	Scandentia		Tupaiidae	*Tupaia belangeri*	16.5	2.3	10.3	126.2	2,852.3
	Primates	Strepsirrhini	Cheirogaleidae	*Cheirogaleus medius*	39.9	1.7	5.7	134.7	1,425.6
			Lorisidae	*Perodicticus potto*	24.5	2.6	7.9	139.7	2009.5
			Lemuridae	*Lemur catta*	23.0	2.3	6.7	199.3	1,793.7
		Tarsiiformes	Tarsiidae	*Tarsius bancanus*	23.8	3.6	18.8	277.9	6,827.4
		Haplorhini, Platyrrhini	Atelidae	*Alouatta caraya*	29.3	3.0	12.2	386.4	7,623.4
			Pitheciidae	*Pithecia pithecia*	20.2	5.4	14.0	445.5	3,701.4
			Callitrichidae	*Cebuella pygmaea*	29.0	4.4	11.6	162.8	3,441.2
				Saguinus imperator	31.0	5.3	12.2	223.5	7,685.6
		Haplorhini, Catarhhini	Cercopithecidae	*Cercocebus agilis*	30.4	2.8	14.3	540.0	14,434.2
				Cercocebus kandti	26.3	2.4	11.4	354.2	7,398.1
				Erythrocebus patas	39.4	2.6	16.2	288.4	11,638.6
				Mandrillus sphynx	23.3	3.6	13.0	364.1	5,043.9
				Macaca fascicularis	42.4	2.0	15.0	282.5	13,157.3
				Macaca mulatta	39.9	4.7	20.3	389.3	7,674.1
				Chlorocebus pygerythrus	46.7				
				Papio ursinus	37.5	5.3	16.3	337.2	4,687.3

Infra-class	Order	Suborder, Parvorder	Family	Species	A	B	C	D	E
			Hominidae	*Gorilla gorilla*	35.8	4.7	21.3	404.0	9,488.4
				Hylobates muelleri	36.6	3.1	22.6	415.3	21,675.1
				Pan paniscus	44.5	3.0	23.9	713.5	44,416.4
				Pan troglodytes	41.6	3.5	26.9	720.0	32,019.6
				Pongo pygmaeus	31.2	3.7	23.9	593.9	28,101.8
				Homo sapiens	32.5	5.1	27.9	593.4	25,220.9
	Chiroptera	Micro-chiroptera	Phyllostomidae	*Carollia perspicillata*	17.8	3.0	8.5	164.5	1,348.5
				Glossophaga soricina	21.0	3.0	6.3	106.9	470.9
		Mega-chiroptera	Pteropodidae	*Epomops franqueti*	14.0	5.0	9.8	213.1	1,026.3
				Megaloglossus woermanni	18.0	2.3	5.3	55.2	343.7
				Rousettus aegyptiacus	23.0	2.3	3.8	84.5	437.9
	Eulipotyphla		Erinaceidae	*Atelerix frontalis*	15.5				
	Carnivora	Feliformia	Felidae	*Felis catus*	14.2	1.3	4.0	131.3	1,273.3
				Panthera tigris	17.2	2.2	7.2	111.9	1,536.9
		Musteloidea	Mustelidae	*Mustela putorius*	18.8	3.1	8.0	187.1	1,619.9
		Caniformia	Ailuridae	*Ailurus fulgens*	19.6	2.3	7.0	119.5	1,572.1
	Artiodactyla	Ruminantia	Bovidae	*Ovis aries*	13.2	2.3	8.3	180.9	4,998.1
		Whippo-morpha	Hippopotamidae	*Hippopotamus amphibius*	17.6	2.1	5.0	205.0	1,485.4
		Cetacea	Balaenopteridae	*Balaenoptera acutorostrata*	20.4	2.1	7.4	202.0	3,175.7
			Phocoenidae	*Phocoena phocoena*	18.0	1.7	6.1	78.7	1,211.8

Column A = # cells/mm; Column B = # primary processes; Column C = # total processes; Column D = Total length; Column E = Complexity.